Biomass Conversion and Biorefinery (2025) 15:2199–2221
https://doi.org/10.1007/s13399-023-05138-0

REVIEW ARTICLE

Syntheses and applications of iron-based functional materials for bioenergy production: a review

Xin Li[1] · Lijun Wang[1,2] · Abolghasem Shahbazi[1,2]

Received: 3 August 2023 / Revised: 30 October 2023 / Accepted: 13 November 2023 / Published online: 2 December 2023

Abstract

The earth abundant and environmentally friendly element iron (Fe) forms various functional materials of metallic iron, iron oxides, iron carbides, natural iron ore, and iron-based metallic-organic frameworks. The Fe-based materials have been intensively studied as oxygen carriers, catalysts, adsorbents, and additives in bioenergy production. This review was to provide a fundamental understanding of the syntheses and characteristics of various Fe-based materials for further enhancing their functionalities and facilitating their applications in various bioenergy conversion processes. The syntheses, characteristics, and applications of various iron-based materials for bioenergy conversion published in peer-reviewed articles were first reviewed. The challenges and perspectives of the wide applications of those functional materials in bioenergy conversion were then discussed. The functionalities, stability, and reactivity of Fe-based materials depend on their structures and redox phases. Furthermore, the phase and composition of iron compounds change in a process. More research is needed to analyze the complex phase and composition changes during their applications, and study the type of iron precursors, synthesizing conditions, and the use of promoters and supports to improve their performance in bioenergy conversion. More studies are also needed to develop multifunctional Fe-based materials to be used for multi-duties in a biorefinery and develop green processes to biologically, economically, and sustainably produce those functional materials at a large scale.

Keywords Iron · Bioenergy · Additives · Oxygen carrier · Catalysts · Adsorbent

1 Introduction

Lignocellulosic biomass which typically contains 35–50 wt% cellulose, 20–35 wt% hemicellulose, and 10–25 wt% lignin is the most abundantly available raw materials on earth for bioenergy production [1]. Many biorefining processes have been developed to convert lignocellulosic biomass into various energy products based on the physical nature and chemical composition of biomass feedstocks and the demands for the types of energy products. The biomass conversion technologies can be mainly classified into three types: thermochemical conversion (i.e., combustion, gasification, pyrolysis), biological conversion (i.e., fermentation, anaerobic digestion, bio-photochemical process), and chemical conversion (i.e., transesterification, hydrogenation). During thermochemical conversion, the inherent energy of biomass is either released directly as heat via combustion or transferred into other favorable products in the form of solid charcoal, liquid bio-oil, or syngas via pyrolysis or gasification. Biological conversion utilizes whole cells such as bacteria or enzymes from cells to convert biomass into biogas, bioethanol, biochemicals, and bioelectricity. Chemical processes of biomass feedstocks are mainly used in the production of diesel from several resources including fats, oil crops, and waste oil via transesterification [1].

Iron (Fe) which consists of 32.1% of the mass of the earth has been intensively studied as a functional material for enhancing bioenergy conversion. α-Fe, γ-Fe, δ-Fe, and ε-Fe are the four known allotropes in the pure form (Fe^0). Iron can lose a variable number of electrons to form various compounds with a wide range of oxidation states. The most common oxidation states are Fe(II) and Fe(III). Higher

✉ Lijun Wang
lwang@ncat.edu

[1] Department of Natural Resources and Environmental Design, North Carolina Agricultural and Technical State University, 1601 East Market Street, Greensboro, NC 27411, USA

[2] Department of Chemical, Biological and Bioengineering, North Carolina Agricultural and Technical State University, 1601 East Market Street, Greensboro, NC 27411, USA

state of Fe(VI) was found in the purple potassium ferrate (K_2FeO_4), while $[FeO_4]^-$ with Fe(VII), along with an Fe(V)peroxo isomer, has also been detected [2]. Fe(IV) is a common intermediate in many biochemical oxidation reactions [3]. Iron-based materials including zero-valent iron (ZVI), iron oxides, and iron carbide have unique characteristics of electron conductivity, magnetism, reduction–oxidation, and biocompatibility. Iron-based materials have been used as additives to improve the performance and recovery of microorganisms in the biological conversion of biomass, catalysts and oxygen carriers in thermochemical conversion of biomass, and adsorbent to capture C O_2 during bioenergy conversion [4–6].

However, there is no published review comprehensively summarizing the syntheses, characteristics, and applications of various iron-based materials in bioenergy conversion. This review was thus focused on the syntheses, characteristics, and applications of various iron-based materials for bioenergy conversion published in peer-reviewed articles. The challenges and perspectives were discussed for the wide applications of iron-based materials in bioenergy conversion. The articles were identified by the keywords "iron," "zero-valent iron," "iron oxides," "magnetite," and "oxygen carrier" together with "bioenergy" in the databases of Science Direct and Google Scholar. The objective of this review was to provide a fundamental understanding of the syntheses and characteristics of various iron-based materials for further enhancing their functionalities and facilitating their applications in various bioenergy conversion processes.

2 Syntheses and characteristics of iron-based functional materials

2.1 Zero-valent iron (ZVI)

ZVI is a readily available, highly effective, inexpensive, and strong reducing agent. It can be oxidized to Fe(II) and Fe(III). Nanoscale ZVI (nZVI) particles have larger reactive surface areas and better injection ability and mobility than microscale ZVI. nZVI particles are traditionally used to decompose organic compounds in wastewater and inactivate microorganisms. However, a proper amount of nZVI can be added to the biological process to enhance the performance of the microorganisms by facilitating interspecies electron transfer and providing the micronutrient iron and other benefits for the conversion of biomass into biofuels [7].

nZVI can be synthesized by physical, chemical, and biological methods [8]. Grinding, abrasion, lithography, and nucleation of iron from a homogeneous solution or gas are traditional physical methods to produce nZVI. The physical methods do not require any toxic reagents and can be used to produce nZVI at a large scale. However, nZVI particles produced by the physical methods usually have irregular shapes and a high tendency of aggregation. Chemical reduction of Fe^{3+} ions by $NaBh_4$, reduction of FeOOH and Fe_2O_3 by H_2 at an elevated temperature, and decomposition of $Fe(CO)_5$ in organic solvents can produce nZVI particles. Electrolysis of a solution containing F e^{2+}/Fe^{3+} salts can deposit atoms of iron on the cathode to produce nZVI. The main challenge of the electrochemical method is its high tendency of aggregation and formation of clusters. Ultrasound can be used to control the particle size of nZVI during the physical and chemical processes [8]. Physical and chemical methods for producing nZVI need high temperature, high pressure, toxic chemicals, and high-energy inputs. Plant extracts such as citrus extract and microorganisms can be used as reducing agents to synthesize nZVI particles, which is not only environmentally friendly but also inexpensive. A polyphenolic solution obtained by heating plant extracts in water can be mixed with a solution of F e^{2+} to reduce the iron ions to nZVI. One of the drawbacks of the green synthesis is the formation of iron oxides as well due to the incomplete reduction of iron to nZVI. nZVI particles are usually not stable in the environment due to the high tendency of agglomeration and oxidation. Various methods such as surface coating, emulsification, and deposition of nZVI on a carrier have been used to modify nZVI for various applications [8].

2.2 Fe(II) and Fe(III) oxides

Iron oxides of F e_2O_3, Fe_3O_4, and FeO are abundant in the earth's crust. However, those natural iron cores contain a lot of impurities which affect their target functionalities in bioenergy conversion. Various synthetic approaches have been studied to produce iron oxides with desirable oxidation states, formula, and particle sizes. Iron oxides are usually synthesized by precipitation, co-precipitation, and impregnation methods.

Precipitation by adding a sodium carbonate or urea alkaline solution to an Fe(III) salt solution such as iron nitrate is the most common method for the synthesis of iron oxides. This method can produce supported iron oxides with a higher degree of reduction and higher Fe-loading than other approaches. The precipitated iron oxides are further dried and calcinated [9]. There are mainly three steps in the preparation of the iron oxides in the industry: (1) thermal decomposition of iron-containing solid salts, (2) oxidation of the metallic iron to oxides by organic oxidizer (e.g., nitrobenzene), (3) precipitation of soluble iron salts with

alkali salts, followed by oxidation [10]. Another way is to mix an iron salt solution and an alkaline solution concurrently at constant pH. Promoters such as Cu can be added to the iron oxides by adding promoter metal salts such as $Cu(NO_3)_2$ and iron salt $Fe(NO_3)_3$ together in an alkali solution such as Na_2CO_3 for co-precipitation to enhance the performance of the iron oxides [11].

Another method to prepare iron oxide precursor is via impregnation, which is mostly used on carbon-based supports such as activated carbon (AC) [12], carbon sphere [13], carbon nanotubes (CNTs) [14], and carbon nanofibers (CNFs) [15]. The iron loading of the impregnation methods is normally lower than 30 wt.% in order to achieve well-distributed iron particles [16]. Ultrasonic agitation has been used to increase the metal loading (40–50wt %) and dispersion during impregnation [12]. The research found that the precursor of ammonium iron citrate showed better iron dispersion on a support than iron nitrate [17]. Furthermore, traceable amounts of sodium and sulfur purity in the ammonium iron citrate can serve as a promoter of the iron oxides [18].

2.3 Magnetic iron oxides

Magnetic iron oxides typically consist of magnetite (Fe_3O_4) and/or maghemite (γ-Fe_2O_3). As magnetic iron oxides exhibit ferromagnetism, they can be easily recovered using an external magnetic field. Magnetic iron oxides that are cheap and easily recovered have been studied as catalysts for bioenergy conversion and carriers for immobilizing biocatalysts and harvesting microalgae [19].

The magnetic iron oxide particles can be synthesized using the methods discussed in Sect. 2.2. The magnetic characteristics of the iron oxides are determined by the type of iron oxides, which are affected by the iron precursors and processing conditions of temperature and pH value. The optimization and control of the temperature for preparing magnetic iron oxides are critical because the iron oxides can change the phase during the synthesis at various temperatures [20]. Surface modification of those magnetic iron oxide particles is usually needed for specific applications [19].

2.4 Iron-based metal–organic frameworks (MOFs)

Metal–organic frameworks (MOFs) are a type of crystalline porous materials formed by linking a metal ion or metal ion cluster with an organic linker. Iron-based MOFs that are iron-containing porous materials have been used as adsorbents and catalysts in bioenergy conversion. MOFs are traditionally synthesized by solvo(hydro)thermal methods. When soluble MOF precursors in a solvent are heated to reach their critical concentrations, self-assembled nucleation will start to produce crystals to form crystalline porous metal-MOFs. The temperature should be controlled to obtain a suitable crystalline form of MOFs but avoid the degradation of the reticular networks [21].

As traditional methods require large amount of solvents and energy inputs, several new MOF synthesis methods including mechanochemical, electrochemical, dry-gel, diffusion, and plasma syntheses have been studied to produce MOFs at a large scale in an economic and environmentally friendly way. During mechanochemical synthesis, mechanical energy via grinding induces bond breakage and chemical transformations of the precursors to form a threedimensional structure of MOFs within a very short time. Electrochemical synthesis has been used to produce MOF film and coatings by electrolyzing a reaction medium containing metal ion and organic linker at a room temperature. The metal can also be used as an anode directly. Spray synthesis consists of three steps: atomization of the precursor solutions using compressed air or nitrogen, drying the atomized droplets suspended in the gas at a certain temperature, and formation of porous MOFs when the amount of the solvent in the droplets decreases. Dry-gel synthesis uses steam to assist in the conversion of the precursor sols to crystalline porous coordination compounds. Microwave, ultrasound and plasma are also used to facilitate the transformation of the precursors to MOF structures [21].

2.5 Iron carbides

Iron carbides are a compound of iron and carbon with various compositions from η-Fe_2C to o-Fe_7C_3 reported in the literature, which have unique electronic, catalysis, and magnetic properties. Iron carbides have been considered as one of the most important Fisher-Tropsch synthesis catalysts. Iron carbides can be produced by the carbonization of ironbased MOFs as the precursor. An Fe@C catalyst was prepared by pyrolyzing Basolite F300, which is a type of FeMOF precursor [22]. In the synthesis, the Fe to C ratio was adjusted by adding furfuryl alcohol as a carbon source. This approach achieved a high iron loading of 25–38 wt% meanwhile retaining the good dispersion of the active iron carbide phase. The Fe@C catalyst exhibited nearly two orders of magnitude more active than the benchmark catalyst, a carbon nanofiber-supported iron catalyst. Such a remarkably high activity of Fe@C was related to a higher degree of carburization of iron [22].

2.6 Iron–nitrogen dual-doped carbon (Fe–N/C)

The iron–nitrogen dual-doped carbon (Fe–N/C) has been intensively studied to develop catalysts for oxygen reduction reaction in fuel cells in the past two decades [23]. The typical synthesis method of Fe–N-C is through pyrolyzing the widely available precursors comprising iron salts, nitrogenrich molecules, and carbon precursors under a high temperature in either N_2 or NH_3. The carbon component in the catalysts serves as both the conductive support and the host of active moieties [24–26]. In general, ideal electrocatalysts should possess good electrical conductivity, hierarchical pore structure, large specific surface area, and competent active sites. Therefore, the iron-containing precursors are normally introduced in various carbonaceous materials with these properties, including activated carbon, graphene, carbon nanotube (CNT), conducting polymers, and porous carbons [24–26]. Figure 1 shows three synthesis procedures of Fe–N/C catalysts which were reported recently, each of which represents a typical strategy for introducing heteroatoms (Fe and N) into the carbon materials.

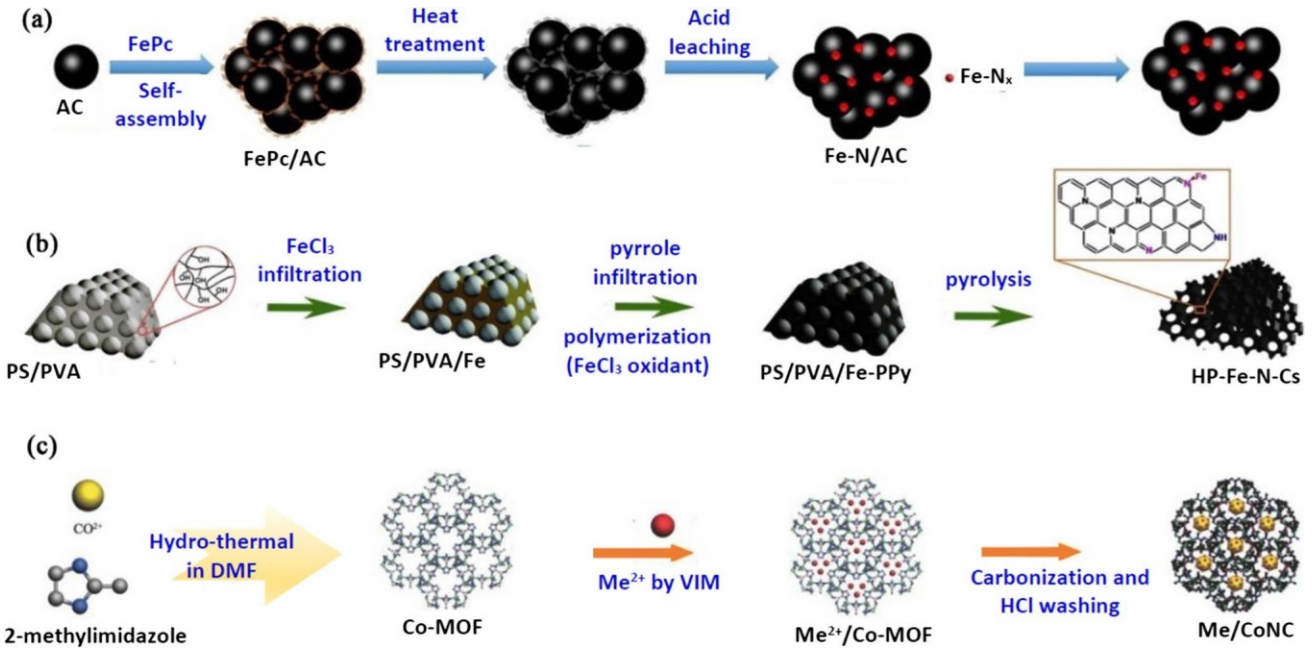

Figure 1a shows the evaporation-induced self-assembly method for preparing an iron–nitrogen/activated carbon (Fe–N/AC) by pyrolyzing FePc-coated AC [24]. In this case, the interaction between the iron macrocycle compounds and carbon planes was done through π-π stacking; thus, the agglomeration of macrocycle complexes can be inhibited to some extent. Similarly, other carbonaceous materials such as graphene oxide (GO) and ordered mesoporous carbon (OMC) can also be used as the support in this strategy. The combination of high specific surface area, ordered mesoporous structure, and well-dispersed Fe-N_x moieties offers it an outstanding ORR activity, as compared with commercial Pt/C. But the high cost of macrocyclic compounds prevents this method from large-scale synthesis and industrial application [24].

Figure 1b shows an example of coupling conducting polymers with iron cation for an electrocatalyst. The conducting polymers include polypyrrole (PPy) and polyaniline (PANI). Su et al. synthesized the hierarchical porous iron and nitrogen co-doped carbons (HP–Fe–N–Cs) by using PPy as a nitrogen source and poly(vinyl alcohol) (PVA) hydrogel-based composites as in-situ templates [25]. The abundance of hydroxyls on PVA allows for an easy adsorption of metal ions and thus contributes to the infiltration procedure. As PANI has a higher content of N, it is usually used to achieve more Fe-N_x active sites. The formation of a hierarchical porous structure could be realized by introducing $ZnCl_2$ and $LiCl_2$ mixture during the pyrolysis [27] or in the NH_3 atmosphere [28]. Besides conducting polymers, other N-containing polymers such as polyimide (PI) were also used as the precursors. Upon pyrolysis, PI can be converted to N-doped carbon materials, and the structure of PI can be regulated by choosing different dianhydride and diamine monomers [29].

Figure 1c shows the strategy for the synthesis of Fe–N/C electrocatalysts from MOF precursors [26]. Co-MOF with 2-methylimidazole as the linker (N source) was synthesized and then loaded with various metals (M-Co-MOF) including Fe, Ni, Zn, and Cu. The metal-loaded Co-MOF was carbonized in the N_2 atmosphere to obtain a M-Co–N/C catalyst. However, the results showed that the Fe-Co–N/C catalyst had a lower activity than other metals in the ORR catalysis and was not even comparable to the commercial Pt/C catalysts [26].

Fig. 1 Schematic of the synthesis procedure of (**a**) Fe–N/C catalysts by pyrolyzing FePc-coated activated carbon. Reproduced from Ref. [24]. Copyright (2018) Elsevier. **b** hierarchical porous iron and nitrogen co-doped carbons by coupling polypyrrole with iron cation. Reproduced from Ref. [25]. Copyright (2014) Elsevier. **c** metal-Co–N/C catalysts using MOF as the precursor. Reproduced from Ref. [26]. Copyright (2015) Wiley

3 Applications and improvement of iron-based functional materials for bioenergy conversion

3.1 Iron-based oxygen carriers for combusting and gasifying biomass

3.1.1 Biomass chemical looping combustion and gasification

A set of reduction–oxidation can form a chemical loop process (CLP) in which looping materials circulate, transform, and regenerate cyclically to convert carbonaceous feedstock such as biomass into a combination of heat, electricity, fuels, and chemicals. CLPs have become a promising technology for efficient biomass conversion and possible integration with carbon capture and storage [30]. Iron oxides such as Fe_2O_3 can be used as an oxygen carrier (OC) in the reduction–oxidation cycles of chemical looping combustion (CLC) as shown in Fig. 2a and chemical looping gasification (CLG) in Fig. 2b.

The reactions that occur in a typical CLC of biomass ($C_nH_{2m}O_p$) are as follows, where Eq. (1) is the overall reaction that occurs in a combustor, and Eq. (2) shows the regeneration of OCs:

$$C_nH_{2m}O_p + (2n+m-p)Me_xO_y \rightarrow nCO_2 + mH_2O + (2n+m-p)Me_xO_{y-1} \quad (1)$$

$$(2n+m-p)Me_xO_{y-1} + (n+0.5m-0.5p)O_2 \rightarrow (2n+m-p)Me_xO_y \quad (2)$$

Me_xO_y and Me_xO_{y-1} are the oxidized and reduced forms of an OC. In the combustor, the OC reacts with the biomass to produce CO_2 and H_2O and releases heat while simultaneously being reduced to Me_xO_{y-1}. The Me_xO_{y-1} is then transferred to the regenerator, where it is oxidized with air to be recycled. The reactions for the CLG are similar to CLC, except that the biomass is partially oxidized in a fuel reactor to produce CO and H_2, expressed by Eq. (3). It should be noted that in some cases, H_2O or CO_2 could be added to the gasifier to enhance syngas production due to the occurrence of steam reforming by Eq. (4) and dry reforming by Eq. (5).

$$C_nH_{2m}O_p + (n-p)MexOy \rightarrow nCO + mH_2 + (n-p)Me_xO_{y-1} \quad (3)$$

$$C_nH_{2m}O_p + (n-p)H_2O \rightarrow nCO + (m+n-p)H_2 \quad (4)$$

$$C_nH_{2m} + nCO_2 \rightarrow 2nCO + mH_2 \quad (5)$$

3.1.2 Fe-based OC properties and redox mechanism

Ideal OCs in CLPs should have the ability to transport oxygen in a cyclic process and to undergo multiple cycles with chemical, thermal, and physical stability. The reduction/ oxidation potentials of different iron oxides are determined by their positions in a modified Ellingham diagram given in Fig. 3, which depicts the standard Gibbs free energies of reactions as a function of temperature. The diagram consists of three important zones outlined by three lines, which correspond to three reactions related to CO_2, H_2, and CO. The location of the OC lines indicates the potential to fully or partially oxidize the fuel [31]. For example, iron-based OCs, Fe_2O_3, and Fe_3O_4 both fall in the combustion zone, indicating strong oxidizing potentials and capability for full and partial oxidation of fuels. FeO in the syngas production zone can only produce CO or H_2, and the yielded syngas cannot be further oxidized, which makes it a good candidate for gasification. Ellingham diagram provides only the theoretical guidance for the selection of OCs. Practical determination of the OCs should be a combined consideration of reaction kinetics, reactants mixing ratio, contact time, and process design.

Figure 4 shows the mechanism for the oxygen carrier's interaction with the reducing agent of H_2 and the oxidizing agent of O_2 in a complete reduction–oxidation cycle

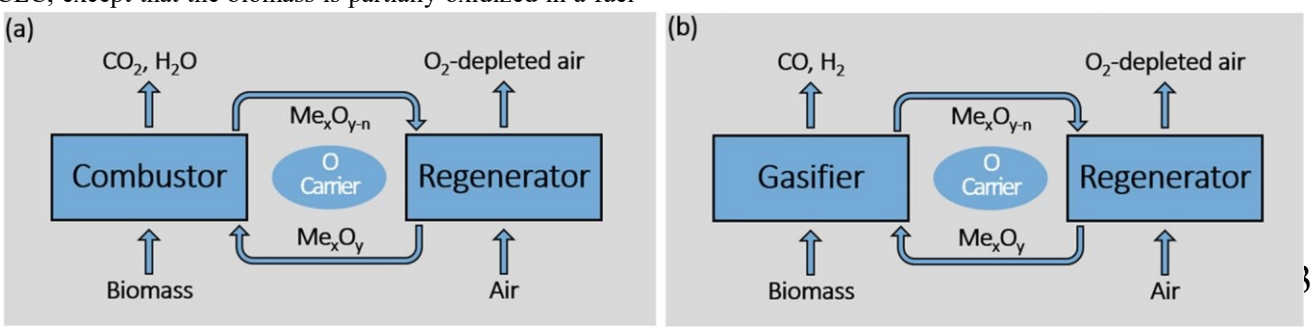

Fig. 2 Schematic principles of (**a**) biomass chemical looping combustion (BCLC), (**b**) biomass chemical looping gasification (BCLG)

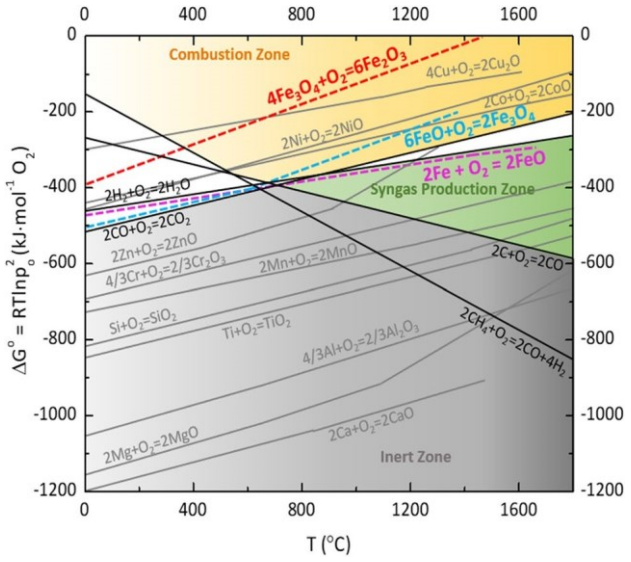

Fig. 3 Modified Ellingham diagram for comparing various oxygen carriers for their applications in chemical looping combustion and gasification. Reproduced from Ref. [31]

[32]. In the reduction step (Fig. 4a), the lattice oxygen in the OC turns into active oxygen species (e.g., O^{2-}, O^{-}, and O_2^{-}) by absorbing thermal energy at a high temperature. Due to the oxygen chemical potential gradient, these oxygen anions diffuse from the bulk to the surface of the OC particle. The oxygen species react with the reducing agents such as H_2, biomass, and biofuels on the particle surface to generate various products. Reversely, during the oxidation step (reduction of the reactant gas), surface exchange and reaction occur with the generated oxygen ions and electron holes, which subsequently diffuse inward and combine with oxygen vacancies in the bulk (Fig. 4b).

Iron oxides are considered good OCs owing to their low cost, high mechanical strength, high melting points, and being environmentally benign. Oxygen transport capacity (R_o), which is the maximum oxygen transport capability of an OC between its fully oxidized and reduced forms, is:

$$R_o = \frac{m_o - m_r}{m_o} \quad (6)$$

where m_o is the mass of the fully oxidized OC and m_r is the mass of the reduced OC.

Figure 5a shows the comparison of R_o values of different OCs. Both Fe_2O_3 and Fe_3O_4 ranked among the top OCs with outstanding oxygen transport ability. The relatively high melting points of iron oxides shown in Fig. 5b offer an inherent thermal stability in the CLPs. Figure 5c summarizes and compares the major features of various OCs [33]. Fe-based OCs show the low reactivity to CH_4 and moderate reactivity to H_2 and CO. Fe-based OCs have no tendency for carbon formation or sulfide/sulfate formation. The disadvantage of iron oxides is the agglomeration issue associated with the formation of magnetite. In spite of its relatively low reactivity, Fe-based OCs are still regarded as good materials for CLPs.

3.1.3 Improvements of iron-based OCs

Supports The agglomeration is a serious issue of Fe-based OCs which leads to the de-fluidization in fluidized bed reactors and deactivation of the OCs. Fe-based OCs were reported to have agglomeration problems when magnetite

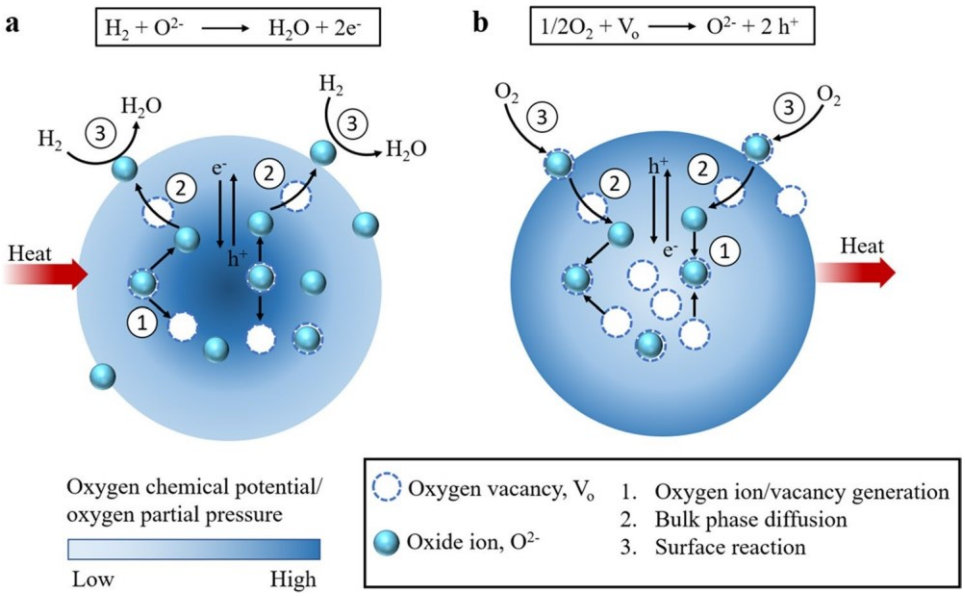

Fig. 4 Intereaction of OC redox cycle. particles with H**a** The O_2 and O_2^- on the 2 in a surface of metal oxide particles is removed by H_2 to form H_2O leading to the migration of more O^{2-} to the surface. **b** The particle is oxidized by O_2, and the electrons move to the surface, making O^{2-} fill the oxygen vacancy (V_O). Reproduced from Ref. [32]

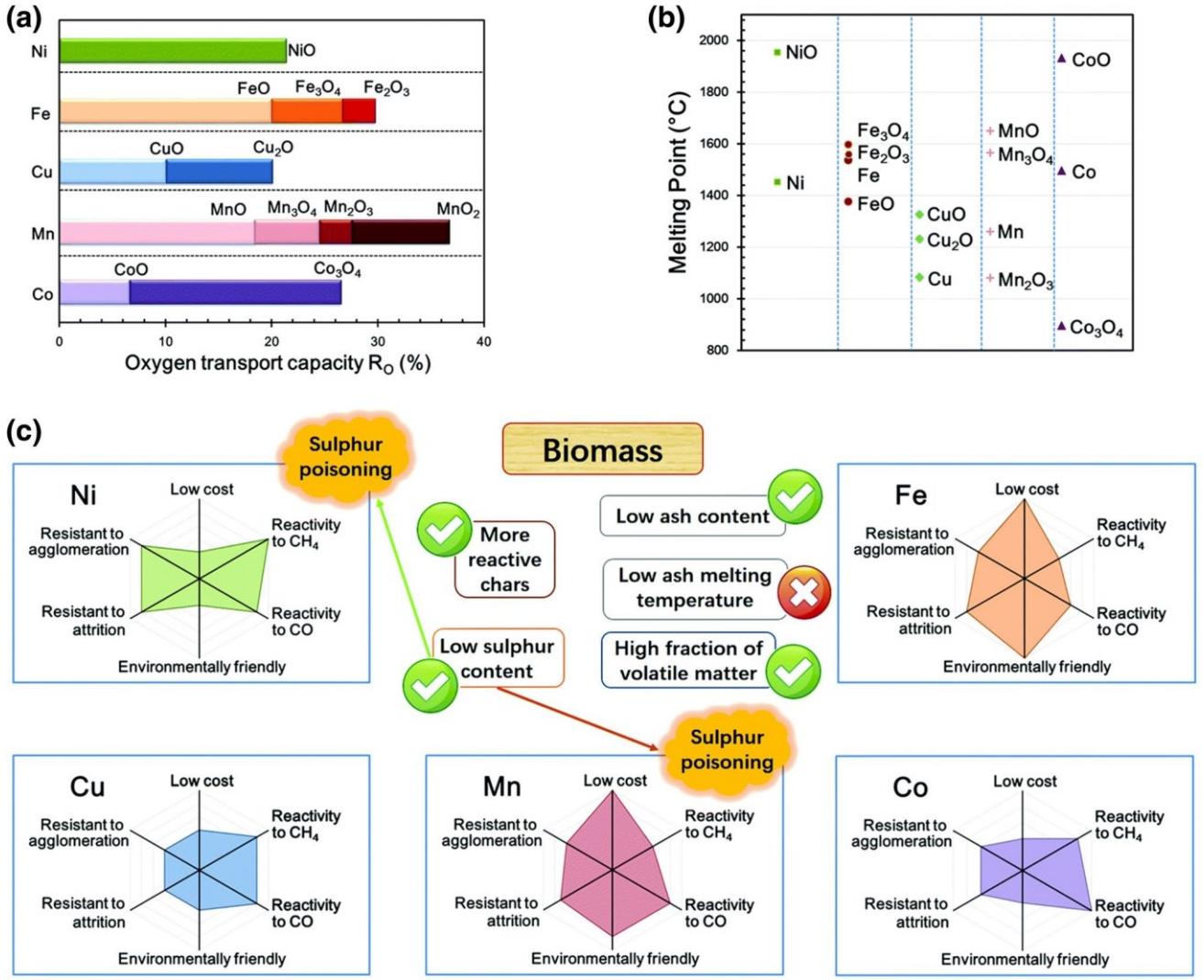

Fig. 5 Comparison of Ni, Fe, Cu, Mn, and Co-based OCs: **a** oxygen transport capacity, **b** melting point, and **c** cost, reactivity, and resistance to agglomeration or attrition. Adapted from Ref. [33]. Copyright (2017) Royal Society of Chemistry

(Fe_3O_4) transforms into wustite (FeO) at a high temperature [34]. Therefore, iron oxides are generally synthesized on supporting materials for better stability and higher strength by mitigating the agglomeration. Support materials sometimes also enhance the reactivity of the iron oxides due to their physiochemical properties or the interaction with the iron oxides. T iO_2 has been reported to be a good support for OCs due to its low cost and good reactivity. Either synthesized or obtained natural ore, TiO_2-supported Fe-based OCs usually exist in the form of ilmenite—$FeTiO_3$. The mechanical mixture of F e_2O_3 and T iO_2 can eventually generate ilmenite at a high temperature as an OC [35]. The formation of $FeTiO_3$ was also achieved in Fe-based OCs prepared with the incipient wet impregnation method, which was subjected to a high temperature of 900 °C [36]. The notable improvement of the iron oxide on T iO_2 support (represented by $FeTiO_3$) might be the result of a lower energy barrier for O^{2-} migration within the dense solid

phase, thereby enhancing the O^{2-} diffusivity [37]. Al_2O_3 has also been used as the support for Fe-OCs. It is found that mixing Fe_2O_3 with Al_2O_3 exhibited an enhanced activity in both CLC and CLG [38]. It was reported that the optimum ratio of F e_2O_3 to A l_2O_3 in the mixture was 6:4 for its best performance in producing hydrogen in a CLG [35]. However, the iron oxide supported on Al_2O_3 using the co-precipitation method showed poor reactivity and stability, owing to the formation of $FeAl_2O_4$ after multiple cycles [39]. So far, conventional support of SiO_2 was rarely used to support Fe-based OCs, possibly because it easily reacts with iron oxide to form inactive silicates [40]. Recently, our research group employed silicalite-1, a polymorph of S iO_2 with MFI zeolite framework, as the Fe-based
OC support. This novel multifunctional OC was found to be resistant to the formation of silicate, as compared with conventional SiO_2, and exhibited a good performance in tar decomposition and high adsorption capacity for C O_2 [41]. Various carbon sources including raw biomass, biochar, and activated carbon were used to produce carbon supported iron oxygen carrier/catalyst for biomass gasification [42]. It was found that the type of carbon sources had significant effect on the phase of iron. The use of biomass as a carbon source and potassium as a promoter could increase F e^{2+} and Fe^0 contents of the catalyst, which could remove 80% tar and double syngas yields during catalytic biomass gasification, compared to the control of biomass pyrolysis without the use of any oxygen carrier/catalyst [42].

Mixing with other OC metals To take the advantages of more than one metals or even generate certain synergies, OCs composed of mixed metal oxides are usually used in CLPs. Copper oxide is usually added to the iron-based OCs to increase its reactivity in a CLG process [43, 44]. It was reported that Cu-Fe OCs with a high Cu content prepared by the sol–gel combustion synthesis method showed better reactivity in the gasification of sawdust. The optimal molar ratio of CuO/Fe_2O_3 was 1:1 in terms of overall syngas quality, carbon conversion, and tar yield [43]. The addition of the CuO phase in the OC contributed to the formation of the porous structure. Cu-Fe mechanical mixtures also exhibited significant improvement in carbon conversion and C O_2 conversion in the CLC of the sewage sludge process, due to the formation of $CuFeO_2$. Moreover, this mixed oxide also favors the conversion of NO to N_2, hence decreasing the NO emission [45]. MnFe-based OCs manufactured via the spray drying method and sintered at 950 °C produce a spinel of $(Mn_{0.77}Fe_{0.23})_3O_4$ [46]. This type of mixed oxide exhibits high reactivity with gases (i.e., H $_2$, CO, C H_4, and O $_2$) and high oxygen transport capacity during redox cycles between oxidized form, $(Mn_{0.77}Fe_{0.23})_3O_4$, and reduced form, $(Mn_{0.77}Fe_{0.23})O$. Although the investigation was carried out with coal as feedstock, but Mn-Fe OCs are also promising in biomass-based CLPs due to their proven efficiency in the combustion of solid fuels. N iFe_2O_4 spinel was used in a biomass-CLG coupled with water/CO_2-splitting process, where $NiFe_2O_4$ spinel provided an oxygen source for the biomass gasification to generate syngas, and then the reduced metal oxide was re-oxidized by introducing water or CO_2 to replenish its lattice oxygen, producing hydrogen or carbon monoxide [47]. The presence of N iFe_2O_4 OC promotes biomass conversion, especially biochar conversion at an elevated temperature. Fe_2O_3-Al_2O_3 mixture impregnated by NiO exhibited stable reactivity and high resistivity to sintering in CLG of sawdust. The gasification efficiency reached up to 70.48% under the optimized condition [48]. $CeFeO_3$ was another mixed OC that exhibited good reactivity in the coupled reforming of pyrolytic gas from the biomass and CO_2 splitting process. $CeFeO_3$ contributes to the creation of oxygen vacancies and lattice oxygen transfer [49]. The improvement is attributed to the resultant oxygen anion vacancy when two cerium cations are replaced with two iron cations. Another cause is the defects (e.g., shear planes) created between two metal oxides, which increase the rate of oxygen anion transfer through the oxygen carrier framework [50].

Perovskite structure Perovskite is a type of complex metal oxide with a general formula of A BO_3, in which A is usually a lanthanide ion and/or alkaline earth metal while B is a transition metal ion, e.g., Fe. The ideal perovskite structure is in the form of BO6 octahedral, with A occupying the center. The perovskite structure is often written as A $BO_{3-\delta}$, where δ expresses the amount of oxygen deficiency [51]. An Fe-containing perovskite shows high thermal stability, good mechanical properties, and good reactivity. The citrate method is widely used to synthesize perovskites. Stoichiometric amounts corresponding to salts as precursors (e.g., La, Ca, Fe, Sr) are dissolved in deionized water, followed by the addition of a citric acid solution. The slurry is dried and then calcined at 900–1200 °C [52]. Co-precipitation of the metal salts in a precipitant agent is another method to synthesize perovskites [53].

Perovskites can also be synthesized by the rapid solidstate synthesis (SSR) method, in which powder oxide or carbonates mixture of the B-site and A-metal are mixed followed by pelletization and annealing/solid-state reaction [54]. There are extensive studies on the La- and Ca-based perovskites as oxygen carriers in gas-fuel CLPs for hydrogen generation [55], reforming [52], and combustion [56]. Labased perovskite is broadly used in methane combustion due to its high activity, facilitated oxygen

mobility, and thermal stability, especially L $eFeO_3$ and its doped counterparts [57]. Ca-based perovskite's advantages include its low cost and tendency to be slightly exothermic in the fuel reactor [58]. It is also promising for chemical looping oxygen-uncoupling processes, which are kinetically more efficient [56]. While Co or Mn as the B-site cations are suggested to be the most promising materials for complete oxidation of hydrocarbons, Fe is preferential for selective oxidation [59]. Fe is employed as the dopant to substitute for the original B-site cations to improve the perovskite performances [56]. The addition of alkali and alkaline earth metals can change the phases of iron-based oxygen carriers and thus their applications in CLC and CLG. Research showed that iron-based OCs modified by K, Na, or Cu are appropriate for CLC, and OCs modified by Ca or Mn are appropriate for GLG. Unlike Ni and Cu, the K, Ca, and Na are not oxidizable, the oxygencarrying rate of the modified OCs decreased after loading with K, Ca, and Na, which lead to the reduction of Fe_2O_3 to lower iron oxides FeO [60].

3.2 Iron-based catalysts for the production of liquid fuels from syngas

3.2.1 Fischer–Tropsch synthesis (FTS) of liquid fuels from syngas

FTS is an exothermic catalytic process which converts syngas (a mixture of CO and H_2) to a wide range of hydrocarbons by a set of polymerization reactions [61]:

$$n\mathrm{CO}+2n\mathrm{H_2}\rightarrow \mathrm{C}n\mathrm{H_{2n}}+n\mathrm{H_2O} \quad (7)$$

$$n\mathrm{CO}+(2n+1)\mathrm{H_2}\rightarrow \mathrm{C}n\mathrm{H_{2n+2}}+n\mathrm{H_2O} \quad (8)$$

Most Group VIII transition metals (Fe, Ru, Os) and several adjacent metals (Co, Rh, Ni, Pt, Pd) are active to catalyze the FTS reactions. However, only Fe and Co are typically utilized in industry, in consideration of their high selectivity to long hydrocarbon chains and the economic feasibility of the overall FTS process [62]. FTS with Ni, Pt, and Pd catalysts produces too much methane. The high cost and limited resources of Ru and Rh hinder their large-scale applications.

3.2.2 Iron-based catalysts for FTS

Fe-based catalysts are gaining more interests not only because of their low cost and abundant availability, but also many other benefits. The stoichiometric H_2/CO ratio of syngas for FTS is 2. As compared with cobalt, Fe-based catalysts have the capability to produce various products such as olefins and alcohols using syngas with a low H_2/CO ratio [63]. Unlike Co-based catalysts, Fe-based catalysts can also catalyze the reversible water − gas shift (WGS) reaction to use CO_2 in the syngas [63, 64]:

$$\mathrm{CO}+\mathrm{H_2O}\leftrightarrow \mathrm{CO_2}+\mathrm{H_2} \quad (9)$$

Therefore, Fe-based catalysts can be used in FTS using syngas containing a large amount of C O_2. Generally, the FTS involving C O_2 conversion occurs at a high temperature and requires a ratio of H $_2$ to C O_x of H $_2/(2\mathrm{CO} + 3\ \mathrm{CO_2}) = 1$ due to the thermodynamic equilibrium of the WGS reaction.

However, Fe-based catalysts face several challenges including low selectivity of olefins or high-carbon chains and high catalyst deactivation rate. The main challenge for an iron-based FTS catalyst is its notoriously high deactivation rate [10]. Therefore, the mechanism and minimization of deactivation have been extensively investigated for the past decades since Fe-based FTS catalysts were introduced.

Among various iron oxides, hydroxides, and oxidehydroxides, hematite (α-Fe_2O_3), magnetite (Fe_3O_4), maghemite (γ-Fe_2O_3), goethite (α-FeOOH), and lepidocrocite (γ-FeOOH) have been reported as important precursors for FTS [65, 66]. Usually, the activated working states of iron during FTS are magnetite and iron carbides while goethite and lepidocrocite belong to a precursor state, and hematite and meghemite belong to an as-prepared state.

3.2.3 Mechanisms of iron oxides as FT catalysts

Iron oxides (Fe_2O_3, Fe_3O_4, and FeO) are the main precursors of iron-based FTS catalysts. The following two reduction reactions occur depending on the reducing agent and the activation conditions during FTS with iron-based catalysts:

$$\mathrm{Fe_xO_y}+y\mathrm{H_2}\rightarrow x\mathrm{Fe}+y\mathrm{H_2O} \quad (10)$$

$$\mathrm{Fe_xO_y}+y\mathrm{CO}\rightarrow x\mathrm{Fe}+y\mathrm{CO_2} \quad (11)$$

Subsequently, dissociation of CO takes place on the metallic iron surface active site (represented by *) when it is adsorbed. Then, the adsorbed carbon species can react with the metallic iron to form iron carbide species.

$$*+\mathrm{CO}^*\rightarrow \mathrm{C}^*+\mathrm{O}^* \quad (12)$$

$$y\mathrm{C}^*+x\mathrm{Fe}\rightarrow \mathrm{Fe_xC_y} \quad (13)$$

It is generally accepted that magnetite is directly carburized into iron carbides in the CO atmosphere. During this process, oxygen removal and carbon introduction usually occur concurrently by combining the steps of Eqs. (11–13).

Various types of reaction mechanisms such as carbide, CO insertion, and oxygenate have been suggested to produce long hydrocarbon chain products during FTS. Based on the carbide mechanism, the carburization reaction takes place on the iron under FTS conditions due to its very low activation energy. On the other hand, the dissociated CO adsorbed on the iron active site can react with the dissociated hydrogen molecules, also on the iron active site, to form hydrogenated species, CH_x^*, which is the precursor to generate longer hydrocarbon chain products.

$$C^* + xH^* \rightarrow CH^*_x + x^* \quad (14)$$

Carbon deposition is closely related to alkali promoters and reaction temperatures. In the FTS conditions, the carbon deposition usually occurs via the Boudouard reaction:

$$2CO \rightarrow C + CO_2 \quad (15)$$

In the LT-FTS condition, this Boudouard reaction does not occur seriously. When there are many available carbon species on the catalyst surface but the hydrogen atoms are insufficient, the Boudouard reaction will accumulate C and block the active sites and reduce the catalyst activity.

These basic reactions constitute initial transformations which occur on the iron catalyst and reveal that iron carbides play a significant role in FTS. The exact mechanism for the production of hydrocarbons over an iron-based catalyst is so complicated and there is still a debate on it. The carbide mechanism is just one of many explanations of the FTS process, in which it is believed that the iron carbides act as the active sites for the conversion of carbon species to hydrocarbons.

3.2.4 Improvement of iron oxides as FT catalysts

Promoters such as potassium (K) are usually used to increase the performance of iron oxides as FT catalysts. Besides coprecipitation, electrical fusing can well incorporate the promoters (e.g., K_2O, Al_2O_3, and CaO) in the matrix of bulk iron oxide (mainly magnetite) by melting the starting materials between the high-voltage electrodes [67]. Other methods such as argon arc heating, oxyacetylene torch, and induction furnace can also provide melting energy to obtain promoted fused iron catalysts [68].

Iron-based catalysts for FTS come in the form of singlephase or multiphase iron oxide as a precursor supported on various oxide supports, such as Al_2O_3, SiO_2, TiO_2, and carbon-based supports [69]. The precipitated Fe-based and fused Fe-based catalysts are two commercial single-phase catalysts used for low-temperature and high-temperature FTS, respectively. There is an increasing research interest in supported Fe-based FTS catalysts with promoters [70, 71]. It was found that the Fe catalyst supported on MOFs derived porous carbon and promoted with Cu had a Fe loading higher than 37% and high CO conversion and stable FT activity [71].

3.2.5 Iron carbides as FT catalysts

In FTS, the iron carbides are generally transformed from the iron oxide precursors, during the in situ activation treatment or under FT conditions. Table 1 lists the iron carbides with different structures, and these species have been discovered in the FTS catalysts. Although cementite (θ-Fe_3C) and Hägg carbide (χ-Fe_5C_2) are most broadly investigated in FTS studies, hexagonal iron carbides (ε′-$Fe_{2.2}C$, ε-Fe_2C) are also identified in the FTS at relatively low temperatures and/ or low H_2/CO ratios. Unlike θ-Fe_3C and χ-Fe_5C_2, the carbon atoms of which are situated in trigonal prismatic interstices, ε′-$Fe_{2.2}C$ and ε-Fe_2C have carbon atoms situated in octahedral interstices. In most cases, it is believed that, after in situ activation, the FTS catalysts consist of a complex mixture of iron carbides (ε′-$Fe_{2.2}C$, ε-Fe_2C, θ-Fe_3C, and χ-Fe_5C_2), metallic and iron (α-Fe) and iron oxide (Fe_3O_4) [72].

Unlike the catalysts activated by the in situ carbonization from iron oxide precursors, catalysts produced by Fe-MOFs have exhibited high activity and stability in FTS. The MOFderived catalysts are synthesized by pyrolyzing different MOF precursors to form the active sites for FTS, including iron carbides and iron oxides. The precursor is transformed into iron carbide via carbonization. An Fe@C catalyst was prepared by pyrolyzing Basolite F300, which is a type of Fe-MOF precursor [22]. In the synthesis, the Fe to C ratio was adjusted by adding furfuryl alcohol as a carbon source. This new synthesis approach achieved a high iron loading of 25–38 wt% meanwhile retaining the good dispersion of the active iron carbide phase. The novel Fe@C catalyst exhibits nearly two orders of magnitude more active than the benchmark catalyst, a carbon nanofiber-supported iron catalyst. Such a remarkably high activity of Fe@C was related to a higher degree of carburization of iron.

Iron-based catalysts are usually catalyzed at 240–280 °C for low-temperature FTS. However, it was reported that the metallic iron was converted to ε-Fe_2C in a syngas of H_2/CO/N_2 = 64/32/4 at a temperature of 150–200 °C, and the ε-Fe_2C phase exhibited excellent activity, high selectivity to transportation fuels, and remarkable robustness in stability

tests [73]. θ-Fe_3C is produced at temperatures above 300 °C by carbonizing reduced iron in syngas or at 500 °C in methane. However, the carbides prepared in this way are contaminated by free carbon. Another approach to preparing θ-Fe_3C is to react iron powder with the Hägg carbide (χ-Fe_5C_2) at a temperature above 260 °C [10]. It should be noted that θ-Fe_3C is less active than other iron carbides.

Figure 6 shows the formation of different carbide phases predicted by thermodynamic calculations [74]. In the calculation, carbon chemical potential μ_C, as imposed by the gas phase combined with kinetic and entropic effects, was considered a significant variable influencing the stability and reactivity of the iron carbides. In experimentation, heating the catalyst precursor in CO at 5 mL/min and 2 °C/min to 280 °C for 2 h was referred to as the high μ_C pretreatment, while heating the catalyst precursor in a 1% CO/H_2 mixture at 10 mL/min and 2 °C/min to 350 °C for 2 h was referred to as the low μ_C pretreatment.

Table 1 Characteristics of different iron carbides found in FTS catalysts

		Formula	Atom ratio (C:Fe)	Interstitial occupation of C atoms	Carbon wt.%
Hexagonal carbide	ε	Fe_2C	0.50	Octahedral	9.7
	ε′	$Fe_{2.2}C$	0.45	Octahedral	8.9
Hägg carbide	χ	Fe_5C_2	0.40	Trigonal prismatic	7.9
Cementite	θ	Fe_3C	0.33	Trigonal prismatic	6.7

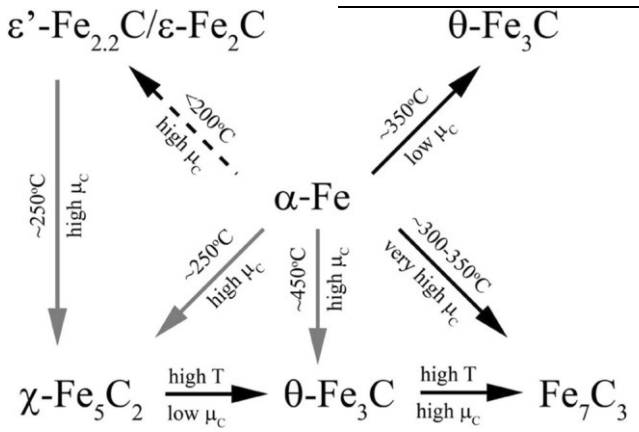

Fig. 6 Schematics of the phase transformation among various iron carbide structures. Gray arrows indicate transformations with significant entropic contributions to the total free energy and the dashed arrow indicates the kinetically inhibited transformation. Adapted from [74]

3.3 Iron-based catalysts for the decomposition of tar in syngas

3.3.1 Tar composition and elimination technologies

The tars that are a complex mixture of aromatic hydrocarbons, oxygen-containing hydrocarbons, and polycyclic aromatic hydrocarbons in the syngas can cause numerous problems for the utilizations of the syngas, such as the cracking in filter pores, the blockage of filter media, and the condensation in cold spots, resulting in serious operational interruptions [75]. Tars contain significant amounts of energy that can be transferred to the fuel gas such as H_2, CO, and CH_4. Tars can be removed and converted by physical, noncatalytic (e.g., thermal cracking), and catalytic processes [76]. Catalytic tar conversion is a technically and economically interesting approach for syngas cleaning as it has the potential to increase conversion efficiencies while simultaneously circumventing the need for the collection and disposal of tars. Catalysts can be mixed with biomass feedstock for in situ catalytic tar conversion during gasification or pyrolysis [75].

Iron-based oxygen carriers can also serve as the catalysts for tar decomposition, and at the same time, they provide oxygen for gasification. A separate reactor can be used to catalytically convert the tar into syngas after gasification. In this case, the tar conversion can occur at operating conditions from gasification. Table 2 summarizes the major reactions during catalytic tar conversion in a downstream reactor, in which C_nH_m and C_xH_y represent heavy and light tars.

Figure 7 shows the types of catalysts used for tar decomposition including several iron minerals-based catalysts and synthetic iron catalysts [76].

3.3.2 Synthetic iron-based catalysts for tar decomposition

There were few studies on synthetic iron catalysts for tar decomposition because the use of iron ore with minimal treatment is more economic. Iron oxide and metallic iron have been studied for the roles of a specific iron phase in catalytic tar decomposition [77] and their kinetics [78]. The

same methods used for the synthesis of iron-based FTS catalysts can be used to prepare an iron-based catalyst for tar decomposition. Several supports such as olivine, dolomite, and Al_2O_3 have been studied to develop iron-based catalyst for catalytic tar decomposition. As Fe has lower activity, its loading on the support is usually 10–30 wt% [79]. There were a lot of research interests in the iron supported on various chars as the tar decomposition catalysts, but the chars were considered a dominant active catalyst component [80, 81].

Table 2 Reactions involved in the catalytic cracking and decomposition of tars, represented by C_nH_m

Reaction type	Reaction equation	Reaction no
Steam reforming	$C_nH_m + nH_2O \rightarrow nCO + (n + 0.5\ m)H_2$	(16)
Steam dealkylation	$C_nH_m + xH_2O \rightarrow C_xH_y + qCO + pH_2$	(17)
Thermal cracking	$C_nH_m \rightarrow C^* + C_xH_y$ + gas	(18)
Hydro cracking	$C_nH_m + (2n - 0.5\ m)H_2 \rightarrow nCH_4$	(19)
Hydro dealkylation	$C_nH_m + xH_2 \rightarrow C_xH_y + qCH_4$	(20)
Dry reforming	$C_nH_m + nCO_2 \rightarrow 2nCO + 0.5mH_2$	(21)
Cracking	$C_nH_{2n+2} + xH_2 \rightarrow C_{n-1}H_{2(n-1)} + CH_4$	(22)
Carbon formation	$C_nH_{2n+2} \rightarrow nC + (n + 1)H_2$	(23)

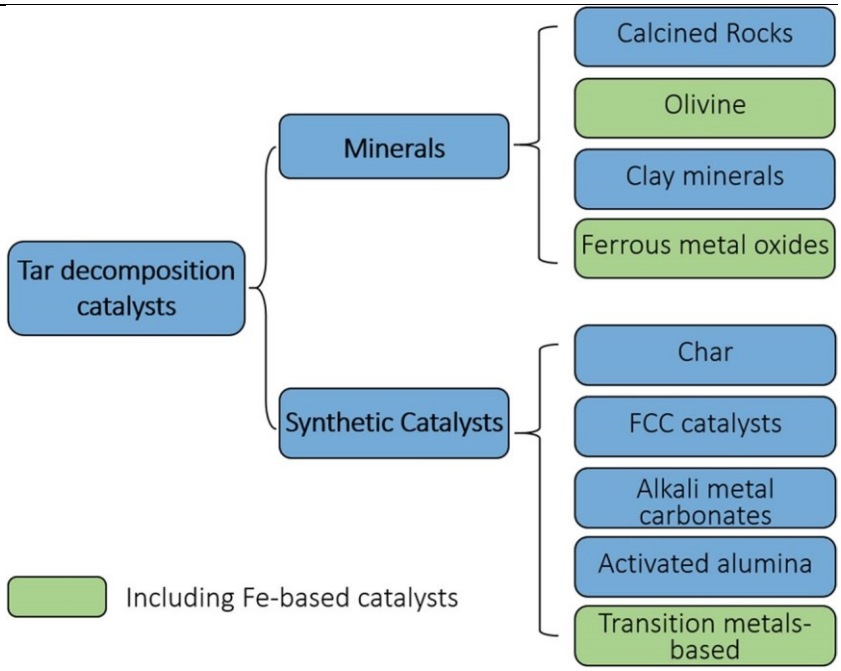

Fig. 7 Classification catalysts used for tar decomposition [76]

activity and reaction mechanism of benzene on iron oxidesilica showed that the catalyst in its reduced form had a high activity toward benzene cracking and a high selectivity toward methane formation [82]. Hydrogen was found to be effective in suppressing the catalyst deactivation [82].

3.3.3 Iron minerals as catalysts for tar decomposition

Iron ores are natural minerals from which metallic iron can be economically extracted. The use of iron ore, directly or with minimal treatment, as the catalysts for tar decomposition is a promising strategy due to the low cost of iron ore and the decent catalytic activity of iron-based catalysts. Minerals containing appreciable amounts of iron can be grouped according to their chemical compositions into oxides (hematite, magnetite, goethite, etc.), carbonates (siderite), sulfides (pyrite), and silicates in which oxide minerals are the most important source. It was reported that the ferrous materials of iron sinter and pellet with a large amount of magnetite (Fe_3O_4) and a small amount of hematite (Fe_2O_3) showed relativity lower activity than dolomite ($CaMg(CO_3)_2$) in catalyzing the decomposition of tar in the temperature range of 700–900 °C [83]. Another study found that hematite had more effect on tar reduction than magnetite [84].

Olivine consists mainly of silicate mineral in which magnesium and iron cations are set in the silicate tetrahedral. The formula to represent natural olivine is $(Mg\ Fe)_2SiO_4$.

Metallic iron is believed to catalyze tar decomposition more actively than the oxides [82]. Iron has the catalytic activity for the reactions involving fuel gases (H_2, CO, CO_2, H_2O) such as the water–gas shift reaction, which is a common secondary reaction in the tar decomposition. Iron is rapidly deactivated in the absence of hydrogen because of coke deposition. Other forms of iron are also reported to have the ability to catalyze gasification reactions, pyrolysis, and tar decomposition. A study on the catalytic cracking

Table 3 gives the compositions of several olivine samples from different resources [85]. The catalytic activity of olivine for tar decomposition is attributed to its magnesite (MgO) and iron oxide (Fe_2O_3). The deactivation of this catalyst is mainly caused by the formation of coke, which covers the active sites and decreases the surface area of the catalyst. Olivine has high mechanical strength at a high temperature like sand and its price is low, which makes it a good bed material and catalyst used in fluidized-bed reactors [86].

It was found that co-feeding hydrogen to steam at a ratio of $P_{H2}/P_{H2O} > 1.5$ could obtain metallic iron on the olivine

surface, which showed the catalytic activity for the steam reforming of toluene as a tar model compound [87]. The study showed that the increase of hydrogen to steam ratio could enhance the decomposition of toluene. At a hydrogen to steam ratio of $P_{H2}/P_{H2O} = 4$, 99.5% of the carbon content in the toluene was converted into CO and C O_2. However, when naphthalene was used as a tar model compound, the presence of H_2 inhibited the decomposition of naphthalene while H_2O and C O_2 could increase the naphthalene decomposition [88].

The catalytic activity of olivine for tar decomposition is relatively low and certain treatments or processing are needed. Iron oxide was added to natural olivine by impregnation to enhance its catalytic activity [89]. The modified olivine with a total 16 wt% iron loading doubled the tar decomposition efficiency. Therefore, the natural olivine impregnated with additional iron oxide can be used as a catalyst for tar reforming and oxygen carrier in a chemical looping process. Simple calcination pretreatment of olivine at 900 °C for 10 h could also significantly improve its catalytic activity for tar removal. It was believed that calcination could lead to the segregation of iron at the surface of olivine for the improved catalytic activity [90]. Biomass-derived ash was used to significantly improve the catalytic activity of olivine for tar decomposition during gasification of biomass due to the formation of a CaO layer on the olivine surface by the ash [91].

Table 3 Chemical compositions of olivine from different resources [85]

	Fe-poor region			Fe-rich region		
SiO_2	40.91	40.90	41.09	40.77	40.48	40.94
TiO_2	0.02	-	-	0.01	0.02	0.02
FeO	8.35	8.00	7.66	9.22	9.14	8.92
NiO	0.33	0.40	0.37	0.34	0.36	0.36
Cr_2O_3	0.00	0.04	0.03	0.01	0.03	0.02
MnO	0.10	0.14	0.16	0.18	0.15	0.14
MgO	50.71	49.52	50.25	49.70	49.92	49.61
CaO	0.02	-	0.02	-	-	-
Total	100.44	99.00	99.58	100.23	100.10	100.01

3.4 *Iron-based sorbents for CO_2 capture during bioenergy conversion*

3.4.1 *CO_2 capture during biomass conversion*

The CO_2 emission in the biomass combustion process is usually considered carbon flux neutral, based on the assumption that CO_2 emitted from biomass combustion equals the C O_2 amount captured in biomass [92]. However, it is of great interest to capture C O_2 from biomass combustion to achieve negative CO_2 emission. The generally high flow rate of flue gas as well as the low CO_2 partial pressure makes it a great challenge to capture CO_2 in flue gas [93]. Although the novel CLC of biomass using calcium oxide as a looping material can produce CO_2-rich flue gas, there is a need for efficient sorbents with a high capacity for adsorbing C O_2. Existing technologies of C O_2 capture are either through physical or chemical adsorption methods. The physical adsorption of CO_2 is fulfilled by the affinity from the solid porous adsorbents, mainly Van der Waals forces, under various conditions, which can be easily released by decompressing or heating the adsorbents. The chemical adsorption is achieved by forming controllable chemical bonds between an adsorbent and C O_2. Two types of iron-based materials were reported as the adsorbents for CO_2 capture which showed promising in bioenergy application: Fe-based metal–organic frameworks and iron oxides.

3.4.2 *Fe-MOFs for CO_2 adsorption*

MOFs mainly capture CO_2 in a physisorptive manner through weak interactions between CO_2 and the pore. In addition, due to their diversity in composition and structures, MOFs can be designed to include open metal sites, basic sites, polar functional groups, controllable pore sizes, various frameworks, and tunable hydrophobicity. These additional sites and features provide extra adsorption capacity and lead to selective adsorption over other gases. The MOFs due to ultra-high surface areas have much higher uptake capacities than other materials. Table 4 summarized CO_2 adsorption capacities of various iron-based MOFs.

An iron-based sodalite-type MOF, Fe-BTT, has the $[Fe_4Cl]^{7+}$ units as the metal clusters in the center and interconnected by triangular BTT^{3-} linkers to form a porous structure [94]. It was reported that this 3-dimensional structure had a BET surface area of 2010 $m^2\ g^{-1}$ and exposed Fe^{2+} coordination sites. The capacity of CO_2 take-up was up to 3.1 mmol/g at 25 °C and 1 bar. Research showed that the open Fe^{2+} cation sites within Fe-BTT served as the extra sites for C O_2 adsorption, making it as a selective

adsorbent for CO 2 over N_2. Another three-dimensional microporous MOF was constructed with F $e_3O(H_2O)_3$ cluster and 2,3,5,6-tetrachloride terephthalic acid (TCDC) ligand [95]. A high density of functional polar groups and open metal sites were detected in this type of MOF, which had a high BET surface area of 1513 m^2 g^{-1}. The highest C O_2 capacity was reported at 5.4 mmol/g at 1 bar and 0 °C. Three MOFs with BDC-containing (BDC = benzene-1,4-dicarboxylate) linkers were investigated for their photocatalytic performance in C O_2 reduction, i.e., MIL-101(Fe), MIL-53(Fe), MIL-88B(Fe). Compared with Fe-BTT and LIFM-26, all these three MOFs had lower CO_2 adsorption capacities of 0.4–1.2 mmol g^{-1}, but their N H_2-functionalized derivatives exhibited 30–48% increase in the C O_2 adsorption, owing to the chemical interaction of the amino group with CO_2.

3.4.3 *Iron oxides for CO_2 adsorption*

Iron oxide other than CaO and MgO provides another option for chemisorptive CO_2 capture. Like a CaO-based adsorbent [96], iron oxide reacts with C O_2 to produce carbonates, which can be heated to release CO_2 and regenerate the iron oxide as shown in Fig. 8. Normally, carbonation reactions are exothermic, and carbonate decomposition reactions are endothermic which allow designing a cyclic process [97]. The attraction of using iron oxide is that, after carbonation and regeneration for several cycles, it can be used for the manufacturing of steel in the same iron-making facility to resolve the high energy consumption and C O_2 emission challenges in the iron-making industry. The potential iron oxide for CO_2 capture is magnetite. Mishra et al. reported a high adsorption capacity of 59.4 mmol g^{-1} at 12 bar and a room temperature for multi-walled carbon nanotubes decorated with Fe_3O_4 nanoparticles [98]. Fe_3O_4 also possesses active sites exposed at the surface (coordinately metal and oxygen sites) that can react with gaseous molecules (H_2, CO_2, O_2, NH_3, CO, H $_2$O) according to acid–base interactions, for Lewis acid or basic sites [99].

Kumar et al. examined a mixture of magnetite (Fe_3O_4) and iron (Fe) as a possible CO_2 sorbent. Figure 8 shows the schematic of their proposed routes: (1) the mixture of magnetite and iron with a molar ratio of 1:1 is used as a CO_2 sorbent; (2) iron carbonates are formed when CO_2 interacts with the sorbent mixture; (3) the separation of unreacted sorbents from the iron carbonates is achieved by applying magnetic field; (4) iron carbonate is heated and decomposed to regenerate magnetite and release CO_2. In this cyclic process, the regenerated magnetite can be used multiple times until its active sites are depleted. In addition, the released pure CO_2 gas can be stored or used for downstream processes.

Both thermodynamic calculations and experiment results showed that the stability of iron carbonate increased with pressure and the decomposition of iron carbonate only occurred at high temperatures for the regeneration of F e_3O_4. Kinetic studies revealed that CO_2 pressure should be elevated above 10 bar to achieve complete carbonation of iron oxides while a minimum of 367 °C was required for the decomposition of the carbonate [100].

Table 4 CO_2 adsorption capacity of various Fe-based MOFs

Adsorbent	Formula	Pressure (bar)	Temperature (°C)	Capacity (mmol Ref g^{-1})	
Fe-BTT	$Fe_3[(Fe_4Cl)_3(BTT)_8(MeOH)_4]_2$	1	25	3.1	[94]
LIFM-26	$Fe_3(TCDC)_3(H_2O)_3$	1	0	5.4	[95]
MIL-101(Fe)	$Fe_3O(OH)(BDC)_3(H_2O)_2$	1	0	1.2	[130]
MIL-53(Fe)	Fe(OH)(BDC)	1	0	0.6	[130]
MIL-88B(Fe)	$Fe_3O(BDC)_3(H_2O)_2$	1	0	0.4	[130]

3.5 Iron-based additives for enhancing the biological conversion of biomass

Iron-based additives can improve the performance of biological processes by supplementing micronutrients, removing inhibitors such as ammonia, and facilitating

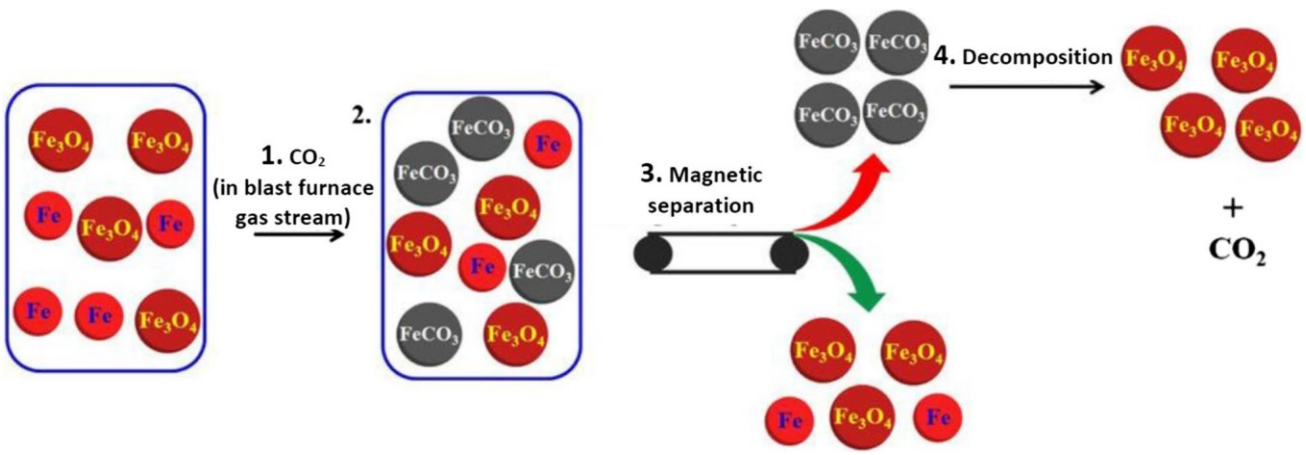

Fig. 8 Schematic of the route for the C O_2 capture using the mixture of magnetite (Fe_3O_4) and iron (Fe) as the adsorbent. Adapted from Ref. [97]. Copyright (2016) Wiley

electron transfer among microorganisms. Fe^{2+} is a component in many enzymes such as hydrogenases in dark fermentation for H_2 production and cell growth. The iron-based additives such as nZVI and iron oxides can increase Fe^{2+} in the aqueous phase to promote the production of target enzymes in cells and the cell growth [101, 102]. The addition of nZVI can reduce the oxidation–reduction potential to create a more favorable anaerobic environment during anaerobic digestion (AD) and dark fermentation [102]. The effects of the addition of iron nanoparticles on the performance of a biological process depend on the type of nanoparticles, concentrations, particle size, and process conditions. The studies reported in the literature were mostly focused on the use of nanomaterials for the enhancement of a specific single function of a biological process such as micronutrient supply and inhibitor removal. More studies are needed to manufacture, characterize, and test multifunctional iron nanocomposite materials for the effective enhancement of the biological performance from various aspects [103].

3.5.1 *nZVI and Fe_3O_4 nanoparticles for enhancing interspecies electron transfer*

Iron-based conductive materials such as nZVI and Fe_3O_4 nanoparticles (Fe_3O_4 NPs) have been used to facilitate interspecies electron transfer among microorganisms in biologic processes such as AD to improve the conversion efficiency [104]. AD is a promising technology used to convert organic solid wastes and wastewater into biogas with four main biological processes: hydrolysis, acidogenesis, acetogenesis, and methanogenesis. However, AD suffers the drawbacks of low conversion efficiency and poor stability [105]. The effects of iron-based additives on the microorganisms are different owing to their physical and chemical properties.

Figure 9a shows the comparison of the methane generation with and without the addition of nZVI. Without nZVI, the methane synthesis during AD is fulfilled through two conventional routes: acetoclastic methanogenesis and hydrogenotrophic methanogenesis, respectively. However, nZVI that tends to release electrons as an electron donor can decrease the redox potential in a biological process. The nZVI acts as the reductant to produce H^+, an important electron transfer carrier utilized by many methanogens for the CO_2 reduction to produce methane. In addition, hydroxyl radical (OH^-) produced by nZVI during AD could be used as an oxidant to increase the biodegradability. The addition of nZVI has shown an increase in the methane and hydrogen production in AD of municipal wastewater and the treatment of industrial wastewater from brewery and sewage plant [106]. Furthermore, nZVI addition also exhibited a better efficiency in the removal of chemical oxygen demand (COD) and in dechlorination [107]. The nZVI is also an effective adsorbent to remove metal pollutants, e.g., Cr(VI) in the wastewater [108].

The main effect of F e_3O_4 NPs in an AD system is to change the direct interspecies electron transfer (DIET) mechanisms [109]. DIET broadly exists in syntrophic processes in which butyrate or hydrogen is used to produce methane. For the systems without F e_3O_4 NPs, the interspecies electron transfer is achieved through hydrogen, formate, and electron transform protein, as shown in Fig. 9b. With Fe_3O_4 NPs in the AD system, the magnetite acts as the electron conduit when the particles are attached to the membrane surface of different cells to accelerate electron transfer between different microorganisms, leading to the improvement of methane generation [110]. Another positive effect is that Fe^{2+}/Fe^{3+} can promote the growth of microorganisms. Other properties including magnetism, adsorptivity, and biocompatibility of Fe_3O_4 NPs can strengthen pollutant digestion efficiency in AD. Fe_3O_4 NPs have been applied in the AD treatment of industrial, municipal, and agricultural wastewater, as well as the solid waste produced from agricultural and municipal activities [110, 111]. The positive effects of Fe_3O_4 NPs on the AD systems were also demonstrated by the increase in the H_2 production and biogas yield [110]. Similar to vZVI, Fe_3O_4 NPs could also remove heavy metal pollutant such as Cr(VI) in the wastewater due to its adsorptive capacity [112].

3.5.2 nZVI additives as a micronutrient of microorganisms

Micronutrient supplements such as Fe, Ni, Mo, Co, W, and Se are crucial cofactors in numerous enzymatic reactions. The lack of some micronutrients can cause poor performance of a biological process. Micronutrient supplements have become an important topic for improving the performance of a biological process. However, excessive concentrations of those micronutrients can lead to the inhibition [113].

As a type of phytoplankton, microalgae require the element Fe, as an essential micronutrient, in their fundamental cellular functions like photosynthesis and respiration [114]. The availability of Fe determines phytoplankton productivity, community structure, and even ecosystem functioning in vast regions of the global ocean. Phytoplankton that is exposed to elevated levels of Fe, especially nZVI is used for various green technologies and marine applications, including the abovementioned wastewater decontamination. However, owing to the high

activity, iron NPs can produce various reactive oxygen species (ROS) via Fenton-type reactions that cause oxidative injury to cells via lipid peroxidation and oxidation of thiol groups on proteins and DNA [115]. Although there are limited studies on the effects of nZVI on the cultivation of microalgae, the mechanisms of its role have not been comprehensively understood.

The type and concentration of iron-based additives can affect not only the growth rate but also the cell compositions. It was found that high concentrations of ferric iron resulted in high lipid content, neutral lipid/total lipid ratio, and saturated fatty acids and 16-C fatty acids, but low cell biomass and polyunsaturated fatty acids in some green microalgae [116]. Another study showed that a mere 5.1 mg L^{-1} nZVI could dramatically increase the cell growth and lipid accumulation in various algae, meanwhile lowering the content of most saturated and unsaturated fatty acids but palmitoleic acid [117]. Experimental results showed when nZVI and Fe-EDTA were used in equal moles in the traditional algal growth media, additive had little effect on the growth, morphology, and cellular lipid content of three investigated marine microalgae (*Tetraselmis suecica*, *Pavolva lutheri*, and *Isochrisis galbana*). The growth of the algae was favored by the nanoparticles in comparison with their bulk analogues [118].

3.5.3 Magnetic iron oxide for harvesting cells

Microorganisms such as microbial and microalgae have been widely used in bioenergy production and biological processes. Magnetotactic cells can be separated and harvested in a magnetic field. One of the applications of magnetic particles is to harvest microalgae. Harvesting technology is crucial in the commercialization of microalgae. The selection of an algae harvesting method is highly dependent on several factors: the physiognomic structure, cell density, algal size, the final moisture content, and the reusability of the culture medium [119]. Conventional harvesting technologies include centrifugation, flocculation by coagulants, precipitation by pH increment, filtration, and flotation [120].

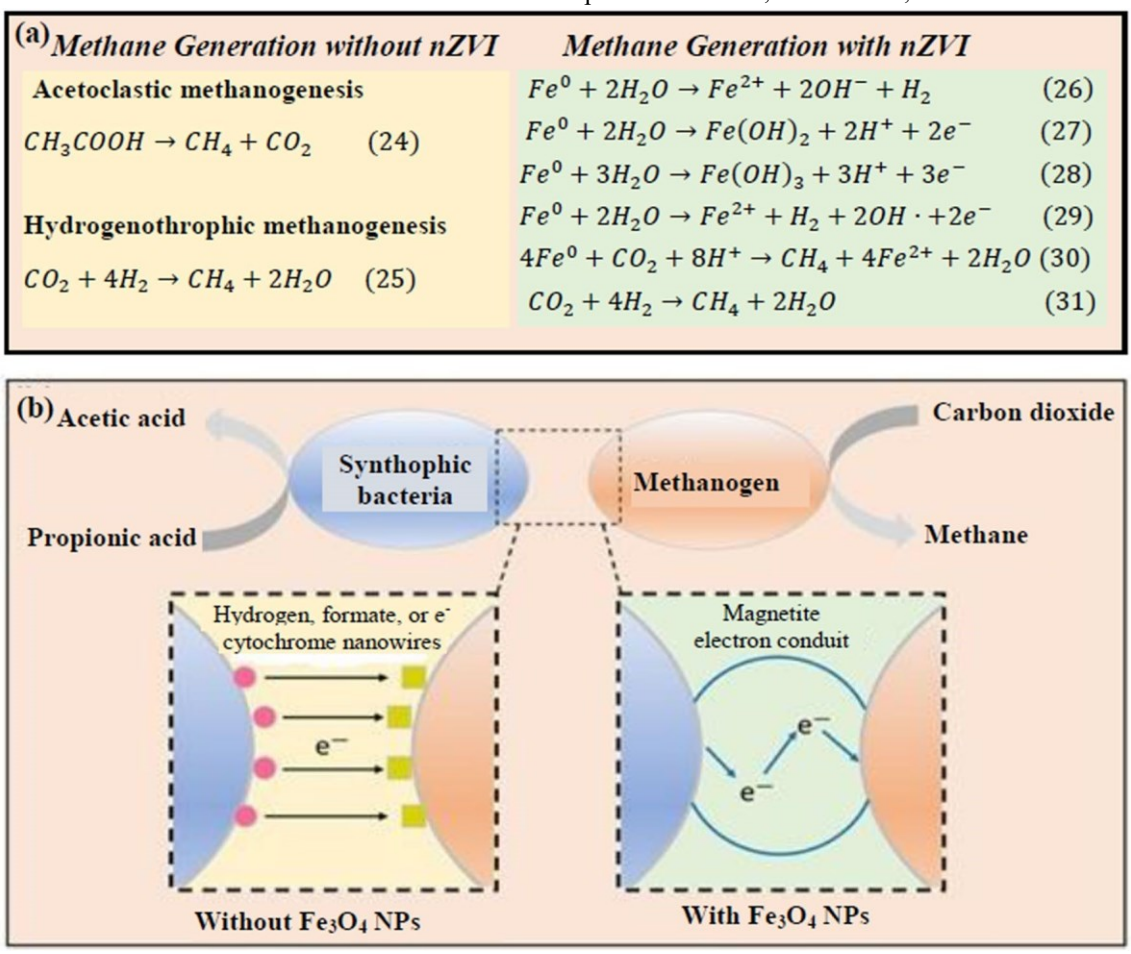

Fig. 9 **a** Comparison of the methane generation with and without nZVI. **b** Comparison of anaerobic digestion with and without F e_3O_4

Magnetophoretic harvesting by tagging algal cells with magnetic particles and then separating them from the culture

medium by an external magnetic field has emerged as an energy-efficient and time-saving technology for microalgal harvesting [121].

Fe_3O_4 NPs are commonly used due to their high specific surface area, superparamagnetism, and biocompatibility. However, tagging magnetic Fe_3O_4 NPs to the negatively charged algal cells requires a specific pH range at which the zeta potential of magnetic nanoparticles shows a positively charged surface. As a result, the coating of cationic materials onto Fe_3O_4 NPs is needed. These cationic materials are normally polymer such as polyethylenimine [122], cationic polyacrylamide [123], poly(diallyldimethylammonium chloride) [124], polyamidoamine [125], (3-aminopropyl) triethoxysilane (APTES), and octyltriethoxysilane (OTES) [126]. Figure 10 shows the procedure of magnetophoretic harvesting of oleaginous microalgae using Fe_3O_4 NPs coated with polyamidoamine (PAMAM) [125]. Table 5 summarizes the main findings of various coating materials for algae harvesting.

3.6 F-N/C composite materials as biocatalysts and bioelectrodes for bioenergy conversion

Microbial fuel cells (MFCs) are bioelectrochemical systems which can generate electricity by electrogenic microorganisms. Electrogenic microorganisms break down organic matter in the electrolyte to produce carbon dioxide, hydrogen ions, and electrons in the anode. Electrons are then transferred along the outer circuit to the cathode, and hydrogen ions diffuse to the cathode through the solution. In the cathode, the oxidant is reduced by the hydrogen ions and electrons. Electrical current is thus produced in such a closed loop [127]. An air-breathing cathode which has a high electrochemical oxygen potential is the most promising configuration. The air-breathing cathode usually consists of an electrode substrate, oxygen reduction reaction (ORR) catalyst layer, and air-diffusion layer as shown in Fig. 11 [127].

The air–cathode catalyst is pivotal in the performance of MFCs because of its role in improving the intrinsic overpotential and poor kinetics of ORR. Although exhibiting the best ORR performance, Pt group metal electrocatalysts have a high cost, low abundance, and easy deactivation in the presence of microbial fuel cell metabolites, hindering them from broad industrial application. So far, numerous non-noble metal electrocatalysts with high cost-effectiveness and excellent catalytic ability have been developed, including Fe–N/C catalysts. Initially, Fe-N_4 macrocycles including iron phthalocyanine (FePc) and ferroporphyrin (FeP) have been investigated as electrocatalysts for MFC. Fe-N_x (the iron atom coordinated with pyridinic or pyrrolic N) and (pyridinic) N-C_x moieties are believed to be the catalytic sites for ORR, but the actual mechanisms are still unclear and debated [128]. Afterwards, plenty of Fe–N/C catalysts were synthesized to introduce Fe and N as dual-dopants on the carbon so that the catalytic sites, i.e., Fe-N_x, and N-C_x, can be generated [129].

4 P erspectives of iron-based functional materials for bioenergy conversion

Various iron-based functional materials of nZVI particles, iron oxides, magnetic iron oxides, iron MOFs, iron carbide, and iron–nitrogen-doped carbon (Fe–N/C) have been studied for bioenergy conversion because of their unique characteristics of electron conductivity, magnetism, reduction–oxidation, and biocompatibility. Iron-based functional materials can be produced by certain treatments of natural iron minerals or syntheses using iron precursors.

Although iron is an abundant and environmentally friendly element on earth, traditional chemical and physical methods for the synthesis of iron-based functional materials require high energy inputs and/or the use of hazardous solvents, which limits the large-scale applications of these iron-based functional materials for bioenergy conversion. More studies are needed to develop green processes using plant extracts, particularly organic wastes, and microorganisms to biologically produce those functional materials at a large scale. More studies are also needed to optimize the processing conditions to control the quality of the target functional materials for specific applications.

Iron oxides that have the advantages of high oxygen transport ability, low cost, and high thermal stability are promising oxygen carriers to supply lattice oxygen for combusting and gasifying biomass. Fe_2O_3 and Fe_3O_4 show strong

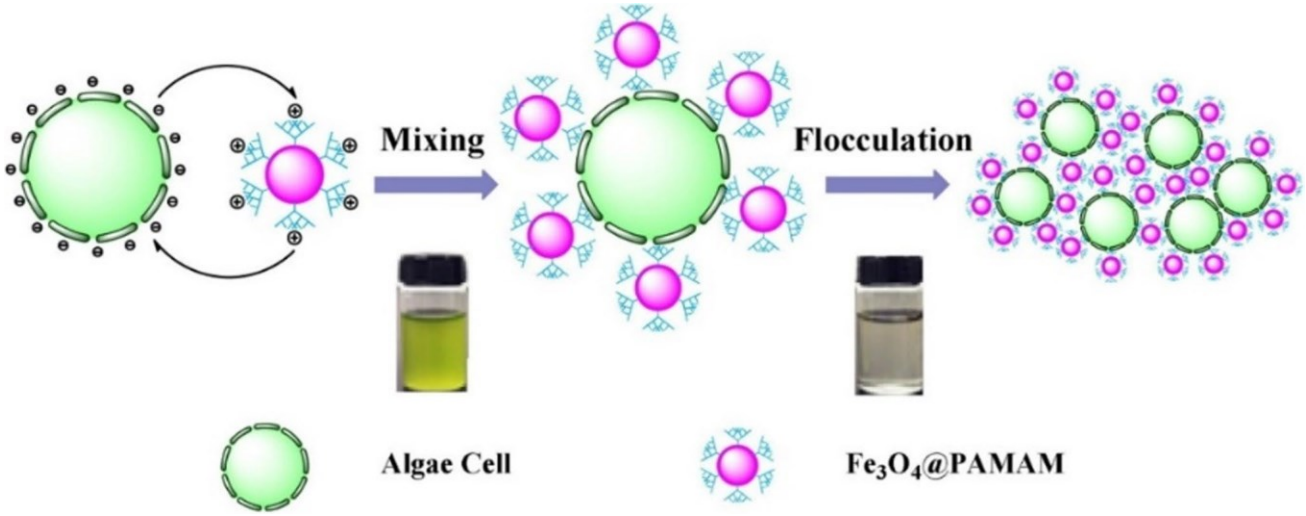

Fig. 10 Schematic of microalgae harvesting using Fe_3O_4 nanoparticles with PAMAM coating. Adapted from Ref. [125]. Copyright (2016) Elsevier

Table 5 Summary of microalgae harvesting using F e_3O_4 NPs with various coating materials

Coating	Microalgae	Significant results	Ref
Polyethylenimine	*Scenedesmus dimorphus*	Harvesting efficiency increased from 60 to 85% as the diameter of coated NPs increased from 9 to 53 nm	[131]
L-arginine	*Chlorella* sp. HQ	Among the ultrasonic approach, long-time mixing approach, and one-step modification approach, the one-step approach presented better harvesting performance	[132]
Polyamidoamine	*Chlorella* sp. HQ	The harvesting was positively correlated with the coating thickness of dendrimer. G3-dMNPs could be regenerated and reused effectively	[125]
Polyethylenimine	*Scenedesmus dimorphus*	Harvesting efficiency was greater under the UV_{365} irradiation than UV_{254}, and increased with the irradiation intensity. Continuous application of the external magnetic field at high strength improved the algal harvesting	[122]
Polyacrylamide	*Botryococcus braunii* *Chlorella ellipsoidea*	A dosage of 25 mg/L for *B. braunii* and 120 mg/L for *C. ellipsoidea* achieved over 95% harvesting efficiency within 10 min as a result of electrostatic attraction and bridging between the magnetic flocculant and the algal cells	[123]
Poly(diallyldimethylammonium chloride)	*Chlorella sp.*	The attached-to strategy was less effective than the immobilized-on strategy as it suffered from agglomeration between the NPs as well as flocculation of the microalgal cells by PDDA	[124]
(3-aminopropyl)triethoxysilane and octyltriethoxysilane	*Chlorella* sp. KR-1	APTES and OTES exhibit cationic charge and enhance lipophilic- [126] ity, respectively. By tuning the APTES/OTES ratio, the magnetic nanoflocculants can be selectively separated from microalgal flocs at the interface of the water and nonpolar organic solvents	

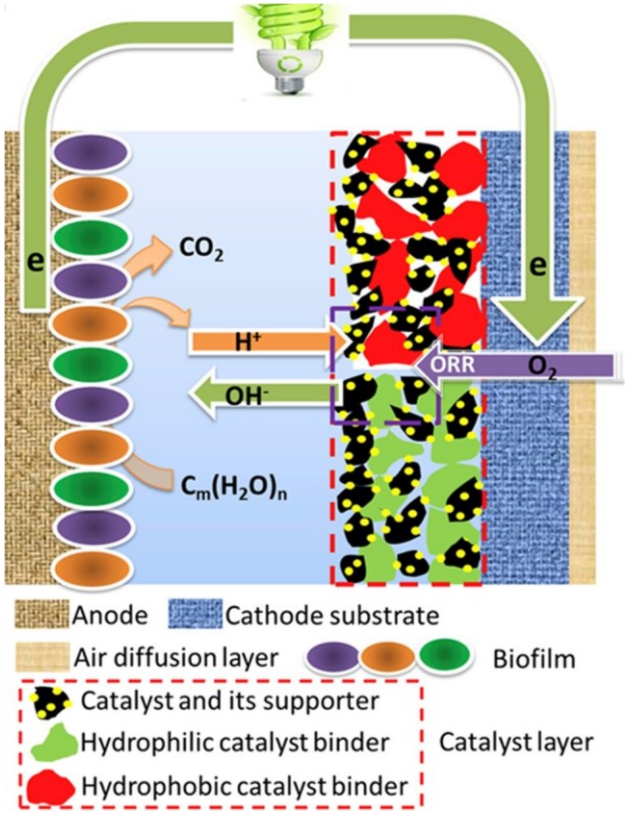

Fig. 11 Schematic of a typical MFC with an anode and air-diffusion cathode, Adapted from Ref. [127]. Copyright (2016) Elsevier

oxidizing potentials and capability for full and partial oxidation of fuels while FeO is a good candidate for gasification as it does not significantly oxidize the product syngas of CO and H_2. The iron oxide OCs face the challenges of low reactivity and high agglomeration. More studies are needed to develop novel supports and promoters to overcome the technical barriers of low reactivity and high agglomeration and control the iron phase for the practical applications of iron oxide-based OCs in bioenergy conversion.

Iron-based catalysts of iron oxides, iron-based MOFs, iron carbide, and Fe–N/C have been widely used in bioenergy conversion, particularly for FTS of liquid fuels from syngas, water–gas shift reaction, cracking tar in syngas, and oxygen reduction in microbial fuel cells. However, the phase of iron, structure, and chemical promoters in the Febased catalysts play the key role in their catalytic activity for specific reactions. The phase of iron is affected by the type of iron precursors, synthesizing conditions, and the use of promoters and supports. More research is needed to study the type of iron precursors, promoters, support, solvents/gases, and synthesizing conditions to optimize and control the phase of the iron in the catalysts and minimize the agglomeration and deviation of the catalysts for their target applications.

Proper structures and phases of iron-based materials can be used to capture C O_2 and selectively produce target products to reduce the separation costs during bioenergy conversion. Fe-based MOFs and iron oxides show excellent capability to adsorb CO_2. More studies are needed to develop iron-based materials that can provide multifunctional duties of oxygen supply, catalysis, and C O_2 sequestration in a biorefinery. Particularly, more studies should be carried out on iron-based composite materials with functionalities for the catalysis, in situ separation, in situ CO_2 sequestration, and selective production of target chemicals in a biorefinery.

Different iron phases play different roles in the functionalities of iron-based materials. However, the phase of iron compounds changes in a process, especially in chemical looping processes. Studies reported in the literature were usually focused on one or a few iron phases and species, which did not provide sufficient information about the interactions and dynamics of various iron compounds in the processes. More research is needed to measure the complex phase changes and analyze the interactions within the iron compound in a specific process.

Iron-based materials particularly zero-valent iron (ZVI) and magnetic iron oxides have been used as additives to improve the performance and recovery of microorganisms in the biological conversion of biomass. However, the effects of the addition of iron nanomaterials on the performance of biological processes depend on the type of nanomaterials, concentrations, particle size, and process conditions. The studies reported in the literature were mostly focused on the use of nanomaterials for the enhancement of a specific single function of a biological process such as micronutrient supply and inhibitor removal. More studies are needed to manufacture, characterize, and test multifunctional iron nanocomposite materials for the effective enhancement of these biological processes from various aspects.

5 Conclusions

Iron (Fe)-based materials of nZVI particles, iron oxides, magnetic iron oxides, iron MOFs, iron carbide, and iron–nitrogen doped carbon (Fe–N/C) have been used as cost effective and environmentally friendly oxygen carriers, catalysts, adsorbent, cell carriers, and additives in bioenergy conversion. The functionalities, stability, and reactivity of iron-based materials depend on their structures and redox phases, which are affected by the type of iron precursors, synthesizing conditions, and the use of promoters and supports. Furthermore, the phase of iron compounds changes in a process. More research is needed to study the phase transition of iron in bioenergy conversion and the type of iron precursors, promoters, supports, solvents/gases, and synthesizing conditions on the phases and structures of iron-based materials to optimize and control the phase of the iron in the functional materials and minimize the agglomeration and deviation of the iron for their target applications. An iron-based material shows multi-functions in bioenergy conversion. More studies are needed to develop iron-based materials that can provide multifunctional duties such as oxygen supply, catalysis, and CO_2 sequestration in a biorefinery. Traditional physical and chemical methods for synthesizing iron-based functional materials require high energy inputs and/or the use of hazardous chemicals. More studies are needed to develop green processes using plant extracts, particularly organic wastes, and microorganisms to biologically produce those functional materials at a large scale.

Bioenergy conversion processes usually generate CO_2. Furthermore, a bioenergy conversion process usually produces a wide range of hydrocarbons, and complex and costly separation processes are required to purify the products.

Author contribution XL: literature survey, investigation, writing—original draft. LW: conceptualization, supervision, literature survey, writing—review and editing. AS: funding acquisition, project administration.

Funding A contribution of North Carolina Agricultural and Technical State University, supported by funds provided by the US National Scientific Foundation (Grant #: HRD-1736173) and the US Department of Agriculture-National Institute of Food and Agriculture (Grant #: NC.X 345–5-22–130-1). Mention of a trade name, proprietary products, or company name is for presentation clarity and does not imply endorsement by the authors or the university.

Data availability This a review paper, whose original files and drafts would be made available upon request.

Declarations

Ethical approval Not applicable.

Competing interests The authors declare no competing interests.

References

1. Wang LJ (2014) Sustainable bioenergy production, CRC Press. Taylor & Francis, Boca Raton, Florida
2. Lu J-B, Jian J, Huang W, Lin H, Li J, Zhou M (2016) Experimental and theoretical identification of the Fe(vii) oxidation state in FeO^{4-}. Phys Chem Chem Phys 18:31125–31131. https://d oi.org/ 10. 1039/ C6CP0 6753K
3. Nam W (2007) High-valent iron(IV)–oxo complexes of heme and non-heme ligands in oxygenation reactions. Acc Chem Res 40:522–531. https:// doi. org/ 10. 1021/ ar700 027f
4. Ye W, Lu J, Ye J, Zhou Y (2020) The effects and mechanisms of zerovalent iron on anaerobic digestion of solid waste: a mini-review. J Clean Prod 278:123567. https:// doi. org/ 10. 1016/j. jclep ro. 2020. 123567
5. Yu Z, Yang Y, Yang S et al (2019) Iron-based oxygen carriers in chemical looping conversions: a review. Carbon Resour Convers 2(1):23–34. https:// doi. org/ 10. 1016/j. crcon. 2018. 11. 004
6. Lahuri AH, Rahim AA, Nordin N, Adnan R, Jaafar NF, TaufiqYap YH (2023) Comparative studies on adsorption isotherm and kinetic for CO2 capture using iron oxide impregnated activated carbon. Catal Today 418:114111. https:// doi. org/ 10. 1016/j. cattod. 2023. 114111
7. Zang Y, Yang Y, Hu Y, Ngo HH, Wang XC, Li Y (2020) Zerovalent iron enhanced anaerobic digestion of pre-concentrated domestic wastewater for bioenergy recovery: Characteristics and mechanisms. Bioresour Technol 310:123441. https://d oi.org/1 0 . 1016/j. biort ech. 2020. 123441
8. Stefaniuk M, Oleszczuk P, Ok YS (2016) Review on nano zerovalent iron (nZVI): from synthesis to environmental applications. Chem Eng J 287:618–632. https:// doi. org/ 10. 1016/j. cej. 2015. 11. 046
9. van Steen E, Prinsloo FF (2007) Comparison of preparation methods for carbon nanotubes supported iron Fischer-Tropsch catalysts. Catal Today 71:327–334. https:// doi. org/ 10. 1016/ S0920- 5861(01) 00459-X
10. de Smit E, Weckhuysen BM (2008) The renaissance of ironbased Fischer-Tropsch synthesis: on the multifaceted catalyst deactivation behaviour. Chem Soc Rev 37:2758–2781. https:// doi. org/ 10. 1039/ B8054 27D
11. Wan H, Wu B, Zhang C, Xiang H, Li Y (2008) Promotional effects of Cu and K on precipitated iron-based catalysts for Fischer-Tropsch synthesis. J Mol Catal A Chem 283:33–42. https:// doi. org/ 10. 1016/j. molca ta. 2007. 12. 013
12. Tian Z, Wang C, Si Z, Ma L, Chen L, Liu Q et al (2017) FischerTropsch synthesis to light olefins over iron-based catalysts supported on $KMnO_4$ modified activated carbon by a facile method. Appl Catal A-Gen 541:50–59. https:// doi. org/ 10. 1016/j. apcata. 2017. 05. 001
13. Chen Q, Liu G, Ding S, Chanmiya Sheikh M, Long D, Yoneyama Y et al (2018) Design of ultra-active iron-based FischerTropsch synthesis catalysts over spherical mesoporous carbon with developed porosity. Chem Eng J 334:714–724. https:// doi. org/ 10. 1016/j. cej. 2017. 10. 093
14. Bahome MC, Jewell LL, Padayachy K, Hildebrandt D, Glasser D, Datye AK et al (2007) Fe-Ru small particle bimetallic catalysts supported on carbon nanotubes for use in Fischer-Tröpsch synthesis. Appl Catal A-Gen 328:243–251. https:// doi. org/ 10. 1016/j. apcata. 2007. 06. 018
15. Xie J, Torres Galvis HM, Koeken ACJ, Kirilin A, Dugulan AI, Ruitenbeek M et al (2016) Size and promoter effects on stability of carbon-nanofiber-supported iron-based Fischer-Tropsch catalysts. ACS Catal 6:4017–4024. https://d oi.org/1 0 .1021 /a cscatal. 6b003 21
16. Cheng K, Kang J, King DL, Subramanian V, Zhou C, Zhang Q et al (2017) Chapter three - advances in catalysis for syngas conversion to hydrocarbons. In: Song C, editor. Advances in Catalysis: Academic Press 125–208.
17. Torres Galvis HM, Bitter JH, Khare CB, Ruitenbeek M, Dugulan AI, de Jong KP (2012) Supported iron nanoparticles as catalysts for sustainable production of lower olefins. Science 335:835–838. https:// doi. org/ 10. 1126/ scien ce. 121561
18. Torres Galvis HM, Bitter JH, Davidian T, Ruitenbeek M, Dugulan AI, de Jong KP (2012) Iron particle size effects for direct production of lower olefins from synthesis gas. J Am Chem Soc 134:16207–16215. https:// doi. org/ 10. 1021/ ja304 958u
19. Li X, Liu B, Lao Y, Wan P, Mao X, Chen F (2020) Efficient magnetic harvesting of microalgae enabled by surface-initiated formation of iron nanoparticles. Chem Eng J 408:127252. https:// doi. org/ 10. 1016/j. cej. 2020. 127252
20. Fatimah I, Fadillah G, Yudha SP (2021) Synthesis of iron-based magnetic nanocomposites: a review. Arab J Chem 14(8):103301. https:// doi. org/ 10. 1016/j. arabjc. 2021. 103301
21. Joseph J, Iftekhar S, Srivastava V, Fallah Z, Zare EN, Sillanpää M (2021) Iron-based metal-organic framework: synthesis, structure and current technologies for water reclamation with deep insight into framework integrity. Chemosphere 284:131171. https:// doi. org/ 10. 1016/j. chemo sphere. 2021. 131171
22. Santos VP, Wezendonk TA, Jaen JJD, Dugulan AI, Nasalevich MA, Islam HU et al (2015) Metal organic framework-mediated synthesis of highly active and stable Fischer-Tropsch catalysts. Nat Commun 6:6451. https:// doi. org/ 10. 1038/ ncomm s7451
23. Muñoz-Becerra K, Venegas R, Duque L, Zagal JH, Recio FJ (2020) Recent advances of Fe–N–C pyrolyzed catalysts for the oxygen reduction reaction. Curr Opin Electrochem 23:154–161. https:// doi. org/ 10. 1016/j. coelec. 2020. 08. 006
24. Liu Y, Fan Y-S, Liu Z-M (2019) Pyrolysis of iron phthalocyanine on activated carbon as highly efficient non-noble metal oxygen reduction catalyst in microbial fuel cells. Chem Eng J 361:416–427. https:// doi. org/ 10. 1016/j. cej. 2018. 12. 105
25. Su Y, Jiang H, Zhu Y, Zou W, Yang X, Chen J et al (2014) Hierarchical porous iron and nitrogen co-doped carbons as efficient oxygen reduction electrocatalysts in neutral media. J Power Sources 265:246–253. https:// doi. org/ 10. 1016/j. jpows our. 2014. 04. 140
26. Tang H, Cai S, Xie S, Wang Z, Tong Y, Pan M et al (2016) Metal–organic-framework-derived dual metal- and nitrogendoped carbon as efficient and robust oxygen reduction reaction catalysts for microbial fuel cells. Adv Sci 3:1500265. https://d oi. org/ 10. 1002/ advs. 20150 0265

27. Ren P, Ci S, Ding Y, Wen Z (2019) Molten-salt-mediated synthesis of porous Fe-containing N-doped carbon as efficient cathode catalysts for microbial fuel cells. Appl Surf Sci 481:1206–1212. https:// doi. org/ 10. 1016/j. apsusc. 2019. 03. 279
28. Tang X, Li H, Du Z, Ng HY (2015) Polyaniline and iron based catalysts as air cathodes for enhanced oxygen reduction in microbial fuel cells. RSC Adv 5:79348–79354. https://d oi.org/1 0 .1039 / C5RA1 6148G
29. Cao W, Lyu L, Deng K, Lu C, Hu C (2020) l-Ascorbic acid oxygen-induced micro-electronic fields over metal-free polyimide for peroxymonosulfate activation to realize efficient multi-pathway destruction of contaminants. J Mater Chem A 8:810–819. https:// doi. org/ 10. 1039/ C9TA1 0284A
30. Fan L-S, Zeng L, Wang W, Luo S (2012) Chemical looping processes for CO_2 capture and carbonaceous fuel conversion – prospect and opportunity. Energ Environ Sci 5:7254–7280. https:// doi. org/ 10. 1039/ C2EE0 3198A
31. Fan L-S, Zeng L, Luo S (2015) Chemical-looping technology platform. AIChE J 61:2–22. https:// doi. org/ 10. 1002/ aic. 14695
32. Zeng L, Cheng Z, Fan JA, Fan L-S, Gong J (2018) Metal oxide redox chemistry for chemical looping processes. Nat Rev Chem 2:349–364. https:// doi. org/ 10. 1038/ s41570- 018- 0046-2
33. Zhao X, Zhou H, Sikarwar VS, Zhao M, Park A-HA, Fennell PS et al (2017) Biomass-based chemical looping technologies: the good, the bad and the future. Energ Environ Sci 10:1885–18910. https:// doi. org/ 10. 1039/ C6EE0 3718F
34. Cho P, Mattisson T, Lyngfelt A (2004) Comparison of iron-, nickel-, copper- and manganese-based oxygen carriers for chemical-looping combustion. Fuel 83:1215–1225. https://d oi.org/1 0 . 1016/j. fuel. 2003. 11. 013
35. Chen S, Shi Q, Xue Z, Sun X, Xiang W (2011) Experimental investigation of chemical-looping hydrogen generation using Al_2O_3 or TiO_2-supported iron oxides in a batch fluidized bed. Int J Hydrog 36:8915–8926. https:// doi. org/ 10. 1016/J. IJHYD ENE. 2011. 04. 204
36. Corbella BM, Palacios JM (2007) Titania-supported iron oxide as oxygen carrier for chemical-looping combustion of methane. Fuel 86:113–122. https:// doi. org/ 10. 1016/j. fuel. 2006. 05. 026
37. Li F, Luo S, Sun Z, Bao X, Fan L-S (2011) Role of metal oxide support in redox reactions of iron oxide for chemical looping applications: experiments and density functional theory calculations. Energy Environ Sci 4:3661–3667. https://d oi.org/1 0 .1039 / C1EE0 1325D
38. Ma Z, Zhang S, Lu Y (2020) Activation mechanism of Fe $_2O_3$-Al_2O_3 oxygen carrier in chemical looping combustion. Energy Fuels 34:16350–16355. https://d oi.org/1 0 .1021 /a cs.energ yfuels. 0c029 67
39. Ma S, Chen S, Soomro A, Xiang W (2017) Effects of CeO_2, ZrO $_2$, and Al_2O_3 supports on iron oxygen carrier for chemical looping hydrogen generation. Energy Fuels 31:8001–8013. https:// doi. org/ 10. 1021/ acs. energ yfuels. 7b011 41
40. Mogorosi RP, Fischer N, Claeys M, van Steen E (2012) Strongmetal–support interaction by molecular design: Fe–silicate interactions in Fischer-Tropsch catalysts. J Catal 289:140–150. https:// doi. org/ 10. 1016/j. jcat. 2012. 02. 002
41. Li X, Wang L, Zhang B, Khajeh A, Shahbazi A (2020) Iron oxide supported on silicalite-1 as a multifunctional material for biomass chemical looping gasification and syngas upgrading. Chem Eng J 401:125943. https:// doi. org/ 10. 1016/j. cej. 2020. 125943
42. Khajeh A, Masoumi S, Wang LJ, Shahbazi A (2023) Effects of various carbon-supported iron catalysts on tar removal efficiency and syngas yield during catalytic biomass gasification. J Environ Chem Eng 11(5):110884. https:// doi. org/ 10. 1016/j. jece. 2023. 110884
43. Niu P, Ma Y, Tian X, Ma J, Zhao H (2018) Chemical looping gasification of biomass: Part I. screening Cu-Fe metal oxides as oxygen carrier and optimizing experimental conditions. Biomass Bioenergy 108:146–156. https:// doi. org/ 10. 1016/j. biomb ioe. 2017. 11. 008
44. Muriungi B, Wang LJ, Shahbazi A (2020) Comparison of bimetallic Fe-Cu and Fe-Ca oxygen carriers for biomass gasification. Energies 13:1–11
45. Niu X, Shen L, Jiang S, Gu H, Xiao J (2016) Combustion performance of sewage sludge in chemical looping combustion with bimetallic Cu–Fe oxygen carrier. Chem Eng J 294:185–192. https:// doi. org/ 10. 1016/j. cej. 2016. 02. 115
46. Pérez-Vega R, Abad A, García-Labiano F, Gayán P, de Diego LF, Izquierdo MT et al (2018) Chemical looping combustion of gaseous and solid fuels with manganese-iron mixed oxide as oxygen carrier. Energy Convers Manag 159:221–231. https://d oi. org/ 10. 1016/j. encon man. 2018. 01. 007
47. He F, Huang Z, Wei G, Zhao K, Wang G, Kong X et al (2019) Biomass chemical-looping gasification coupled with water/CO_2-splitting using $NiFe_2O_4$ as an oxygen carrier. Energy Convers Manag 201:112157. https:// doi. org/ 10. 1016/j. encon man. 2019. 112157
48. Wei G, He F, Zhao Z, Huang Z, Zheng A, Zhao K et al (2015) Performance of Fe–Ni bimetallic oxygen carriers for chemical looping gasification of biomass in a 10 kWth interconnected circulating fluidized bed reactor. Int J Hydrogen 40:16021–16032. https:// doi. org/ 10. 1016/j. ijhyd ene. 2015. 09. 128
49. Wei G, Zhou H, Huang Z, Zheng A, Zhao K, Lin Y et al (2021) Reaction performance of Ce-enhanced hematite oxygen carrier in chemical looping reforming of biomass pyrolyzed gas coupled with CO_2 splitting. Energy 215:119044. https://d oi.org/1 0 .1016 /j. energy. 2020. 119044
50. Tong A, Bayham S, Kathe MV, Zeng L, Luo S, Fan L-S (2014) Iron-based syngas chemical looping process and coal-direct chemical looping process development at Ohio State University. Appl Energ 113:1836–1845. https://d oi.org/1 0 .1016 /j.a penergy. 2013. 05. 024
51. Rydén M, Lyngfelt A, Mattisson T, Chen D, Holmen A, Bjørgum E (2008) Novel oxygen-carrier materials for chemical-looping combustion and chemical-looping reforming; La $_x$Sr$_{1-x}$Fe$_y$Co$_{1-y}$O$_{3-\delta}$ perovskites and mixed-metal oxides of NiO, Fe_2O_3 and M n_3O_4. Int J Greenh Gas Control 2:21–36. https:// doi. org/ 10. 1016/ S1750- 5836(07) 00107-7
52. Nalbandian L, Evdou A, Zaspalis V (2011) L a$_{1-x}$Sr$_x$M$_y$Fe$_{1-y}$O$_{3-\delta}$ perovskites as oxygen-carrier materials for chemical-looping reforming. Int J Hydrogen 36:6657–6670. https:// doi. org/ 10. 1016/j. ijhyd ene. 2011. 02. 146
53. Assirey EAR (2019) Perovskite synthesis, properties and their related biochemical and industrial application. Saudi Pharm J 27:817–829. https:// doi. org/ 10. 1016/j. jsps. 2019. 05. 003
54. Galinsky NL, Huang Y, Shafiefarhood A, Li F (2013) Iron oxide with facilitated O_2– transport for facile fuel oxidation and CO_2 capture in a chemical looping scheme. ACS Sustain Chem Eng 1:364–373. https:// doi. org/ 10. 1021/ sc300 177j
55. Dueso C, Thompson C, Metcalfe I (2015) High-stability, highcapacity oxygen carriers: iron oxide-perovskite composite materials for hydrogen production by chemical looping. Appl Energ

157:382–390. https:// doi. org/ 10. 1016/j. apene rgy. 2015. 05. 062
56. Liu L, Li Z, Li Z, Larring Y, Cai N (2020) Heterogeneous reaction kinetics of a perovskite oxygen carrier for chemical looping combustion coupled with oxygen uncoupling. Chem Eng J 417:128054. https:// doi. org/ 10. 1016/j. cej. 2020. 128054
57. Chang H, Bjørgum E, Mihai O, Yang J, Lein HL, Grande T et al (2020) Effects of oxygen mobility in La–Fe-based perovskites on the catalytic activity and selectivity of methane oxidation. ACS Catal 10:3707–3719. https:// doi. org/ 10. 1021/ acsca tal. 9b051 54
58. Rørmark L, Mørch AB, Wiik K, Stølen S, Grande T (2001) Enthalpies of oxidation of C $aMnO_{3-\delta}$, Ca $_2MnO_{4-\delta}$ and S $rMnO_{3-\delta}$ deduced redox properties. Chem Mater 13:4005–4013. https:// doi. org/ 10. 1021/ cm011 050l
59. Mihai O, Chen D, Holmen A (2012) Chemical looping methane partial oxidation: the effect of the crystal size and O content of $LaFeO_3$. J Catal 293:175–185. https://d oi. org/ 10. 1016/j.j cat. 2012. 06. 022
60. Lin Y, Wang H, Fang S, Jian H, Huan Z, Wei G, Wang X, Zhao Z, Huang H (2022) Chemical looping combustion of lignite using iron ore modified by foreign ions: alkaline-earth and transition metal ions. Fuel 327:125079. https://d oi.org/1 0 .1016 /j.f uel.2022.1 2507 9
61. Rafati M, Wang LJ, Dayton DC, Schimmel K, Kabadi V, Shahbazi A (2017) Techno-economic analysis of production of FisherTropsch liquids via biomass gasification: the effects of FischerTropsch catalysts and natural gas co-feeding. Energ Convers Manag 33:153–166. https:// doi. org/ 10. 1016/j. encon man. 2016. 11. 051
62. van Steen E, Claeys M (2008) Fischer-Tropsch catalysts for the biomass-to-liquid (BTL)-process. Chem Eng Technol 31:655–666. https:// doi. org/ 10. 1002/ ceat. 20080 0067
63. Rafati M, Wang LJ, Shahbazi A (2015) Effect of silica and alumina promoters on co-precipitated Fe-Cu-k based catalysts for the enhancement of CO_2 utilization during Fisher-Tropsch synthesis. J CO2 Util 12:34–42. https:// doi. org/ 10. 1016/j. jcou. 2015. 10. 002
64. Bukur DB, Todic B, Elbashir N (2016) Role of water-gas-shift reaction in Fischer-Tropsch synthesis on iron catalysts: a review. Catal Today 275:66–75. https:// doi. org/ 10. 1016/j. cattod. 2015. 11. 005
65. Cornell RM, Schwertmann U (2003) The iron oxides: structure, properties, reactions, occurrences and uses. John Wiley & Sons
66. Guo H, Barnard AS (2013) Naturally occurring iron oxide nanoparticles: morphology, surface chemistry and environmental stability. J Mater Chem A 1:27–42. https:// doi. org/ 10. 1039/ C2TA0 0523A
67. Larson A, Richardson C (1925) Preparation of fused iron oxide for use as a catalyst. Ind Eng Chem 17:971–972. https:// doi. org/ 10. 1021/ ie501 89a039
68. Zhang J, Sun T, Ding J, Xiao H, Kong F, Chen J (2016) Influences of melting method on fused iron catalysts for Fischer-Tropsch synthesis. RSC Adv 6:60349–60354. https:// doi. org/ 10. 1039/ C6RA0 6772G
69. Chen Y, Wei J, Duyar MS, Ordomsky VV, Khodakov AY, Liu J (2021) Carbon-based catalysts for Fischer-Tropsch synthesis. Chem Soc Rev 50:2337–2366. https:// doi. org/ 10. 1039/ D0CS0 0905A
70. Badoga S, Kamath G, Dalai A (2020) Effects of promoters (mn, mg, co and ni) on the fischer-tropsch activity and selectivity of KCuFe/mesoporous-alumina catalyst. Appl Catal A: General 607:117861. https:// doi. org/ 10. 1016/j. apcata. 2020. 117861
71. Wang A, Luo M, Lü B, Song Y, Li M, Yang Z (2021) Effect of na, cu and ru on metal-organic framework-derived porous carbon supported iron catalyst for Fischer-Tropsch synthesis. Mol Catal 509:111601. https:// doi. org/ 10. 1016/j. mcat. 2021. 111601
72. de Smit E, Beale AM, Nikitenko S, Weckhuysen BM (2009) Local and long range order in promoted iron-based FischerTropsch catalysts: a combined in situ X-ray absorption spectroscopy/wide angle X-ray scattering study. J Catal 262:244–256. https:// doi. org/ 10. 1016/j. jcat. 2008. 12. 021
73. Xu K, Sun B, Lin J, Wen W, Pei Y, Yan S et al (2014) ε-Iron carbide as a low-temperature Fischer-Tropsch synthesis catalyst. Nat Commun 5:5783. https:// doi. org/ 10. 1038/ ncomm s6783
74. de Smit E, Cinquini F, Beale AM, Safonova OV, van Beek W, Sautet P et al (2010) Stability and reactivity of ε−χ−θ iron carbide catalyst phases in Fischer−Tropsch synthesis: controlling μ_C. J Am Chem Soc 132:14928–14941. https:// doi. org/ 10. 1021/ ja105 853q
75. Wang LJ, Weller CL, Hanna MA, Jones DD (2008) Contemporary issues in thermal gasification of biomass and application to electricity and fuel production. Biomass Bioenerg 32:573–581. https:// doi. org/ 10. 1016/j. biomb ioe. 2007. 12. 007
76. Ren J, Liu Y-L, Zhao X-Y, Cao J-P (2020) Biomass thermochemical conversion: a review on tar elimination from biomass catalytic gasification. J Energy Inst 93:1083–1098. https:// doi. org/ 10. 1016/j. joei. 2019. 10. 003
77. Nordgreen T, Liliedahl T, Sjöström K (2006) Metallic iron as a tar breakdown catalyst related to atmospheric, fluidised bed gasification of biomass. Fuel 85:689–694. https:// doi. org/ 10. 1016/j. fuel. 2005. 08. 026
78. Liu Y, Guo F, Li X, Li T, Peng K, Guo C et al (2017) Catalytic effect of iron and nickel on gas formation from fast biomass pyrolysis in a microfluidized bed reactor: a kinetic study. Energy Fuels
31:12278–12287. https://d oi.org/1 0 .1021 /a cs.energy fuels .7 b0221 4
79. Cortazar M, Alvarez J, Olazar L, Santamaria L, Lopez G, Villafan-Vidales HI, Asueta A, Olazar M (2022) Activitiy and stability of different Fe loaded primary catalysts for tar elimination. Fuel 317:123457. https:// doi. org/ 10. 1016/j. fuel. 2022. 123457
80. Min Z, Yimsiri P, Asadullah M, Zhang S, Li C-Z (2011) Catalytic reforming of tar during gasification. Part II. Char as a catalyst or as a catalyst support for tar reforming. Fuel 90:2545–2552. https:// doi. org/ 10. 1016/j. fuel. 2011. 03. 027
81. Kastner JR, Mani S, Juneja A (2015) Catalytic decomposition of tar using iron supported biochar. Fuel Process Technol 130:31–37. https:// doi. org/ 10. 1016/j. fuproc. 2014. 09. 038
82. Tamhankar SS, Tsuchiya K, Riggs JB (1985) Catalytic cracking of benzene on iron oxide-silica: catalyst activity and reaction mechanism. Appl Catal 16:103–121. https:// doi. org/ 10. 1016/ S0166- 9834(00) 84073-7
83. Simell PA, Leppälahti JK, Bredenberg JBS (1992) Catalytic purification of tarry fuel gas with carbonate rocks and ferrous materials. Fuel 71:211–218. https:// doi. org/ 10. 1016/ 0016-2361(92) 90011-C
84. Cypres R, Soudan-Moinet C (1980) Pyrolysis of coal and iron oxides mixtures. 1. Influence of iron oxides on the pyrolysis of coal. Fuel 59:48–54. https:// doi. org/ 10. 1016/ 0016- 2361(80) 90010-1
85. Ando J, Shibata Y, Okajima Y, Kanagawa K, Furusho M, Tomioka N (2001) Striped iron zoning of olivine induced by dislocation creep in deformed peridotites. Nature 414:893–895. https:// doi. org/ 10. 1038/ 41489 3a

86. Devi L, Ptasinski KJ, Janssen FJJG, van Paasen SVB, Bergman PCA, Kiel JHA (2005) Catalytic decomposition of biomass tars: use of dolomite and untreated olivine. Renew Energy 30:565–587. https:// doi. org/ 10. 1016/j. renene. 2004. 07. 014
87. Morin M, Nitsch X, Pécate S, Hémati M (2017) Tar conversion over olivine and sand in a fluidized bed reactor using toluene as model compound. Fuel 209:25–34. https://d oi.org/1 0 .1016 /j.f uel. 2017. 07. 084
88. Devi L, Ptasinski KJ, Janssen FJJG (2005) Decomposition of naphthalene as a biomass tar over pretreated olivine: effect of gas composition, kinetic approach, and reaction scheme. Ind Eng Chem Res 44:9096–9104. https:// doi. org/ 10. 1021/ ie050 801g
89. Virginie M, Adánez J, Courson C, de Diego LF, García-Labiano F, Niznansky D et al (2012) Effect of Fe–olivine on the tar content during biomass gasification in a dual fluidized bed. Appl Catal B-Environ 121–122:214–222. https:// doi. org/ 10. 1016/j. apcatb. 2012. 04. 005
90. Devi L, Craje M, Thüne P, Ptasinski KJ, Janssen FJJG (2005) Olivine as tar removal catalyst for biomass gasifiers: catalyst characterization. Appl Catal A-Gen 294:68–79. https:// doi. org/ 10. 1016/j. apcata. 2005. 07. 044
91. Kuba M, Kirnbauer F, Hofbauer H (2017) Influence of coated olivine on the conversion of intermediate products from decomposition of biomass tars during gasification. Biomass Conv Bioref 7:11–21. https:// doi. org/ 10. 1007/ s13399- 016-0204-z
92. Cherubini F, Peters GP, Berntsen T, Ssromman AH, Hertwich E (2011) CO_2 emissions from biomass combustion for bioenergy: atmospheric decay and contribution to global warming. GCB Bioenergy 3:413–426. https:// doi. org/ 10. 1111/j. 1757- 1707. 2011. 01102.x
93. González AS, Plaza MG, Rubiera F, Pevida C (2013) Sustainable biomass-based carbon adsorbents for post-combustion CO_2 capture. Chem Eng J 230:456–465. https://d oi.org/1 0 .1016 /j.c ej. 2013. 06. 118
94. Sumida K, Horike S, Kaye SS, Herm ZR, Queen WL, Brown CM et al (2010) Hydrogen storage and carbon dioxide capture in an iron-based sodalite-type metal–organic framework (Fe-BTT) discovered via high-throughput methods. Chem Sci 1:184–191. https:// doi. org/ 10. 1039/ C0SC0 0179A
95. Chen C-X, Zheng S-P, Wei Z-W, Cao C-C, Wang H-P, Wang D et al (2017) A robust metal–organic framework combining open metal sites and polar groups for methane purification and CO_2/fluorocarbon capture. Chem Eur J 23:4060–4064. https://d oi.org/ 10. 1002/ chem. 20160 6038
96. Al-Mamoori A, Thakkar H, Li X, Rownaghi AA, Rezaei F (2017) Development of potassium- and sodium-promoted CaO adsorbents for CO_2 capture at high temperatures. Ind Eng Chem Res 56:8292–8300. https:// doi. org/ 10. 1021/ acs. iecr. 7b015 87
97. Kumar S, Drozd V, Durygin A, Saxena SK (2016) Capturing CO_2 emissions in the iron industries using a magnetite–iron mixture. Energy Technol 4:560–564. https://d oi.org/1 0 .1002 /e nte.201500 45 1
98. Mishra AK, Ramaprabhu S (2011) Nano magnetite deco-rated multiwalled carbon nanotubes: a robust nanomaterial for enhanced carbon dioxide adsorption. Energy Environ Sci 4:889–895. https:// doi. org/ 10. 1039/ C0EE0 0076K
99. Alfe M, Ammendola P, Gargiulo V, Raganati F, Chirone R (2015) Magnetite loaded carbon fine particles as low-cost CO_2 adsorbent in a sound assisted fluidized bed. Proc Combust Inst 35:2801–2809. https:// doi. org/ 10. 1016/j. proci. 2014. 06. 037
100. Mora Mendoza EY, Sarmiento Santos A, Vera López E, Drozd V, Durygin A, Chen J et al (2019) Iron oxides as efficient sorbents for CO_2 capture. J Mater Res Technol 8:2944–2956. https:// doi. org/ 10. 1016/j. jmrt. 2019. 05. 002
101. Ren Y, Tang S, Hong F et al (2023) Effects of milli-magnetite on biohydrogen production from potato peels: insight of metabolism mechanisms. Fuel 348:128576. https://d oi.org/1 0 . 1016/j. fuel. 2023. 128576
102. Ren Y, Si B, Liu Z, Jiang W, Zhang Y (2022) Promoting dark fermentation for biohydrogen production: potential roles of iron-based additives. Int J Hydrogen Energy 47(3):1499–1515. https:// doi. org/ 10. 1016/j. ijhyd ene. 2021. 10. 137
103. Salehi B, Wang LJ (2022) Critical review on nanomaterials for enhancing bioconversion and bioremediation of agricultural wastes and wastewater. Energies 15:5387. https:// doi. org/ 10. 3390/ en151 55387
104. Sun J, Rene ER, He Y, Ma W, Hu Q, Qiu B (2023) Carbon, iron, and polymer-based conductive materials for improving methane production in anaerobic wastewater treatment systems: a review on their direct interspecific electron transfer mechanism. Fuel 342:127703. https:// doi. org/ 10. 1016/j. fuel. 2023. 127703
105. Rajagopal R, Massé DI, Singh G (2013) A critical review on inhibition of anaerobic digestion process by excess ammonia. Bioresour Technol 143:632–641. https:// doi. org/ 10. 1016/j. biort ech. 2013. 06. 030
106. Wang Y, Wang D, Fang H (2018) Comparison of enhancement of anaerobic digestion of waste activated sludge through adding nano-zero valent iron and zero valent iron. RSC Adv 8:27181–27190. https:// doi. org/ 10. 1039/ C8RA0 5369C
107. Suanon F, Sun Q, Li M, Cai X, Zhang Y, Yan Y et al (2017) Application of nanoscale zero valent iron and iron powder during sludge anaerobic digestion: impact on methane yield and pharmaceutical and personal care products degradation. J Hazard Mater 321:47–53. https://d oi.org/1 0 .1016 /j.j hazmat.2 016 .08.0 7 6
108. Rovikumar KVG, Argulwar S, Sudakaran SV, Pulimi M, Chandrasekaran N, Mukherjee A (2018) Nano-bio sequential removal of hexavalent chromium using polymer-nZVI composite film and sulfate reducing bacteria under anaerobic condition. Environ Technol Innov 9:122–133. https:// doi. org/ 10. 1016/j. eti. 2017. 11. 006
109. Zhang Z-Z, Cheng Y-F, Bai Y-H, Xu L-Z-J, Xu J-J, Shi Z-J et al (2018) Enhanced effects of maghemite nanoparticles on the flocculent sludge wasted from a high-rate anammox reactor: performance, microbial community and sludge characteristics. Bioresour Technol 250:265–272. https:// doi. org/ 10. 1016/j. biort ech. 2017. 11. 053
110. Zhang J, Lu Y (2016) Conductive Fe_3O_4 nanoparticles accelerate syntrophic methane production from butyrate oxidation in two different lake sediments. Front Microbiol 7. https:// doi. org/ 10. 3389/ fmicb. 2016. 01316
111. Cruz Viggi C, Casale S, Chouchane H, Askri R, Fazi S, Cherif A et al (2019) Magnetite nanoparticles enhance the bioelectrochemical treatment of municipal sewage by facilitating the syntrophic oxidation of volatile fatty acids. J Chem Technol Biotechnol 94:3134–3146. https:// doi. org/ 10. 1002/ jctb. 6120
112. Zhang Y, Li H, Gong L, Dong G, Shen L, Wang Y et al (2017) Nano-sized Fe_2O_3/Fe_3O_4 facilitate anaerobic transformation of hexavalent chromium in soil–water systems. J Environl Sci 57:329–337. https:// doi. org/ 10. 1016/j. jes. 2017. 01. 007
113. Romero-Guiza MS, Vila J, Mata-Alvarez J, Chimenos JM, Astals S (2016) The role of additivies on anaerobic digestion: a review. Renew Sust Energ Rev 58:1486–1499. https://d oi.org/1 0 .1016 /j. rser. 2015. 12. 094

114. Gledhill M, Buck KN (2012) The organic complexation of iron in the marine environment: a review. Front Microbiol 3:69. https:// doi. org/ 10. 3389/ fmicb. 2012. 00069
115. LeBel CP, Ischiropoulos H, Bondy SC (1992) Evaluation of the probe 2′, 7′-dichlorofluorescin as an indicator of reactive oxygen species formation and oxidative stress. Chem Res Toxicol 5:227–231. https:// doi. org/ 10. 1021/ tx000 26a012
116. Huang X, Wei L, Huang Z, Yan J (2014) Effect of high ferric ion concentrations on total lipids and lipid characteristics of Tetraselmis subcordiformis, Nannochloropsis oculata and Pavlova viridis. J Appl Phycol 26:105–114. https://d oi.org/1 0 .1007 / s10811- 013- 0056-x
117. Pádrová K, Lukavský J, Nedbalová L, Čejková A, Cajthaml T, Sigler K et al (2015) Trace concentrations of iron nanoparticles cause overproduction of biomass and lipids during cultivation of cyanobacteria and microalgae. J Appl Phycol 27:1443–1451. https:// doi. org/ 10. 1007/ s10811- 014- 0477-1
118. Kadar E, Rooks P, Lakey C, White DA (2012) The effect of engineered iron nanoparticles on growth and metabolic status of marine microalgae cultures. Sci Total Environ 439:8–17. https:// doi. org/ 10. 1016/j. scito tenv. 2012. 09. 010
119. Singh G, Patidar SK (2018) Microalgae harvesting techniques: a review. J Environ Manag 217:499–508. https://d oi.org/1 0 .1016 /j. jenvm an. 2018. 04. 010
120. Kim J, Yoo G, Lee H, Lim J, Kim K, Kim CW et al (2013) Methods of downstream processing for the production of biodiesel from microalgae. Biotechnol Adv 31:862–876. https:// doi. org/ 10. 1016/j. biote chadv. 2013. 04. 006
121. Prochazkova G, Safarik I, Branyik T (2013) Harvesting microalgae with microwave synthesized magnetic microparticles. Bioresour Technol 130:472–477. https:// doi. org/ 10. 1016/j. biort ech. 2012. 12. 060
122. Ge S, Agbakpe M, Wu Z, Kuang L, Zhang W, Wang X (2015) Influences of surface coating, UV rradiation and magnetic field on the algae removal using magnetite nanoparticles. Environ Sci Technol 49:1190–1196. https:// doi. org/ 10. 1021/ es504 9573
123. Wang S-K, Wang F, Hu Y-R, Stiles AR, Guo C, Liu C-Z (2014) Magnetic flocculant for high efficiency harvesting of microalgal cells. ACS Appl Mater Interfaces 6:109–115. https://d oi.org/1 0 . 1021/ am404 764n
124 . Lim JK, Chieh DCJ, Jalak SA, Toh PY, Yasin NHM, Ng BW et al (2012) Rapid magnetophoretic separation of microalgae. Small 8:1683–1692. https:// doi. org/ 10. 1002/ smll. 20110 2400
125. Wang T, Yang W-L, Hong Y, Hou Y-L (2016) Magnetic nanoparticles grafted with amino-riched dendrimer as magnetic flocculant for efficient harvesting of oleaginous microalgae. Chem Eng J 297:304–314. https:// doi. org/ 10. 1016/j. cej. 2016. 03. 038
126. Lee K, Na J-G, Seo JY, Shim TS, Kim B, Praveenkumar R et al (2015) Magnetic-nanoflocculant-assisted water–nonpolar solvent interface sieve for microalgae harvesting. ACS Appl Mater Interfaces 7:18336–18343. https:// doi. org/ 10. 1021/ acsami. 5b040 98
127. Wang Z, Mahadevan GD, Wu Y, Zhao F (2017) Progress of air-breathing cathode in microbial fuel cells. J Power Sources 356:245–255. https:// doi. org/ 10. 1016/j. jpows our. 2017. 02. 004
128. Erable B, Féron D, Bergel A (2012) Microbial catalysis of the oxygen reduction reaction for microbial fuel cells: a review. Chemsuschem 5:975–987. https:// doi. org/ 10. 1002/ cssc. 20110 0836
129. Zhang M, Ma Z, Song H (2020) Carbon supports on preparing iron-nitrogen dual-doped carbon (Fe-N/C) electrocatalysts for microbial fuel cells: mini-review. Chemosphere 273:128570. https:// doi. org/ 10. 1016/j. chemo sphere. 2020. 128570
130. Wang D, Huang R, Liu W, Sun D, Li Z (2014) Fe-based MOFs for photocatalytic CO_2 reduction: role of coordination unsaturated sites and dual excitation pathways. ACS Catal 4:4254– 4260. https:// doi. org/ 10. 1021/ cs501 169t
131. Ge S, Agbakpe M, Zhang W, Kuang L (2015) Heteroaggregation between PEI-coated magnetic nanoparticles and algae: effect of particle size on algal harvesting efficiency. ACS Appl Mater Interfaces 7:6102–6108. https://d oi.org/1 0 .1021 /a csami. 5b005 72
132. Liu P, Wang T, Yang Z, Hong Y, Xie X, Hou Y (2020) Effects of Fe3O4 nanoparticle fabrication and surface modification on Chlorella sp. harvesting efficiency. Sci Total Environ 704:135286. https:// doi. org/ 10. 1016/j. scito tenv. 2019. 135286